NOAA Technical Report NOS OCS 12

# Hydrodynamic Model Development for the Port of New York/New Jersey Water Level and Current Nowcast/Forecast Model System

Eugene Wei
Manchun Chen

Silver Spring, Maryland
July, 2001


**noaa** National Oceanic and Atmospheric Administration

---

U.S. DEPARTMENT OF COMMERCE
National Ocean Service
Office of Coast Survey
Coast Survey Development Laboratory

Office of Coast Survey
National Ocean Service
National Oceanic and Atmospheric Administration
U.S. Department of Commerce

The Offic of Coast Survey (CS) is the Nation's only official chartmaker. As the oldest United States scientific organization, dating from 1807, this office has a long history. Today it promotes safe navigation by managing the National Oceanic and Atmospheric Administration's (NOAA) nautical chart and oceanographic data collection and information programs.

There are four components of CS:

The Coast Survey Development Laboratory develops new and efficient techniques to accomplish Coast Survey missions and to produce new and improved products and services for the maritime community and other coastal users.

The Marine Chart Division collects marine navigational data to construct and maintain nautical charts, Coast Pilots, and related marine products for the United States.

The Hydrographic Surveys Divisions directs programs for ship and shore-based hydrographic survey units and conducts general hydrographic survey operations.

The Navigation Services Division is the focal point for Coast Survey customer service activities, concentrating predominantly on charting issues, fast-response hydrographic surveys and Coast Pilot updates.

## TABLE OF CONTENTS

## LIST OF FIGURES

## LIST OF TABLES

## 1. INTRODUCTION

A New York/New Jersey (NY/NJ) Harbor water level and current nowcast/forecast model system is under development at NOAA's National Ocean Service (Wei, et. al. , 1998). The hydrodynamic model of the system has been developed based on the Princeton Ocean Model (POM) (Blumberg and Mellor, 1987). Utilizing the near real-time water level and current information from NOS Physical Oceanographic Real-Time System (PORTS) (Bethem and Frey, 1991), the model system will provide the water level and current nowcasts and forecasts to mariners to promote navigational safety and to support oil and hazardous materials spill response activities. Reliable current and water level information is very important in preventing vessel collisions in a heavy traffic port such as NY/NJ Harbor, where the U.S. Coast Guard manages vessel traffic based upon tidal current predictions. In the event of a hazardous materials spill, the real-time and forecast information becomes critical for predicting the spill movement, thus minimizing the environmental damage (Parker, 1996).

The Harbor and Port of New York and New Jersey (Figure 1.1) has a complex geometry with narrow navigation channels interconnecting the regional bays, for example, the Kill Van Kull between the Upper Bay and Newark Bay, the East River between the Long Island Sound and the Upper Bay, the Arthur Kill between the Newark Bay and the Raritan Bay. These channels are important for both safe navigation and hydrodynamics in the Harbor. Current shears and eddies, generated by lateral inertial effects at the junction of channels (e.g., at Bergen Point) and other locations, are important to pilots and ship captains trying to maneuver large oil tankers and cargo ships. Very high horizontal resolution is required for a numerical model to accurately predict the occurrence of eddies and current shears.

Four major river systems provide freshwater to each of the three regional bay; the Raritan River to the Raritan Bay, the Passaic and Hackensack Rivers to the Newark Bay, and the Hudson River to the Upper Bay. Discharges from these rivers, ranging from 3 $m^3 s^{-1}$ in the Hackensack River to 400 $m^3 s^{-1}$ at Hudson River, not only play the major role in the vertical and horizontal density stratification but also contribute to the estuarine circulation throughout this hydrodynamically connected system.

The astronomical tide (predominated by the principal semidiurnal component $M_2$) enters the Bay from the Atlantic Ocean through the entrance, between Sandy Hook and Rockway Point. It brings salty water that passes through The Narrows (the deepest water, 25 m) and the Upper Bay to the Hudson River and reaches up to Albany, New York, more than 100 km from the river mouth. Another branch of water flows past the bend to the Kill Van Kull at Constable, producing a shear flow around the bend, and then into Newark Bay, mixing with fresh water from the Passaic and Hackensack Rivers.

The model is a homogeneous three-dimensional version of Princeton Ocean Model (POM) to resolve water level and three-dimensional velocity. A finer sub-grid model, covering channels and bays critical to navigation, including the Kill van Kull and Bergen Point, has been developed, embedded within and dynamically connected to the coarse grid with a coupling technique. This coupled model has been implemented to produce hourly nowcasts including the near-real-time water level and current information in the Harbor. The model also produces 36 hour forecasts forced with water level forecasts at Sandy Hook and Willets Point from a shelf model and wind forecasts from an atmospheric model.

Chapter 2 describes the hydrodynamic model including governing equations and model grid generation. Coarse and fine grid model coupling techniques are introduced in Chapter 3. Chapter 4 describes one year tidal simulation as a model calibration. Model validation simulations with observed water levels and river flows as the boundary conditions are presented in Chapter 5. A summary is given in Chapter 6.

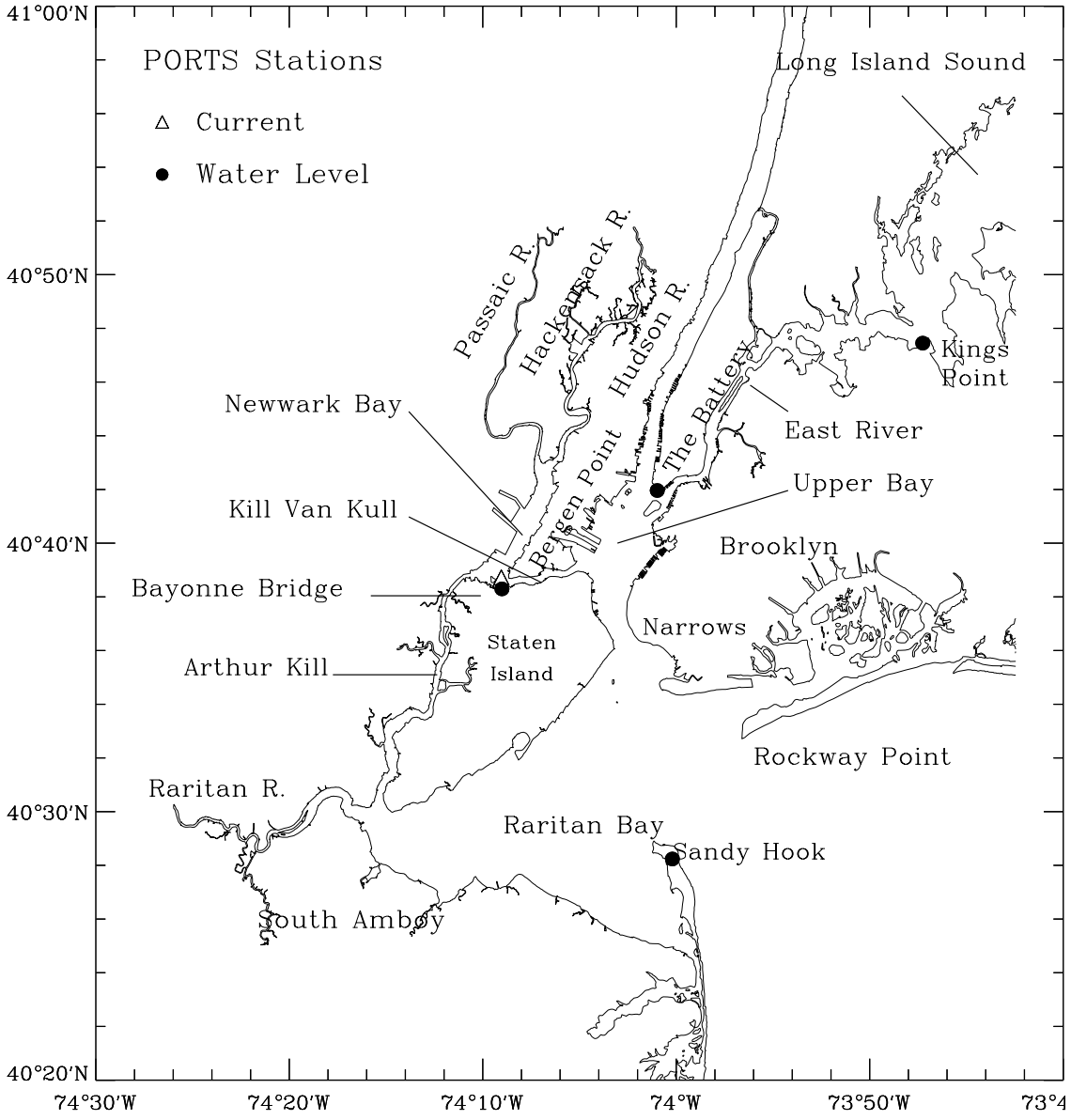


**Figure 1.1.** Map showing New York Harbor and The Port of New York/New Jersey including PORTS stations and major tributaries.

## 2. HYDRODYNAMIC MODEL

### 2.1. Governing Equations

The hydrodynamic model used in the Port of New York/New Jersey water level nowcast/forecast system is developed based on the three-dimensional barotropic version of POM (Blumberg and Mellor, 1987). Since the hydrodynamics of New York Harbor are tidally dominated and the primary goal of the nowcast/forecast system is to focus on the water levels and the currents for navigation safety purposes, the density effect has been neglected in the present model development stage. The governing equations in a sigma coordinate are briefly given as follows. Detailed formulations are contained in Blumberg and Mellor (1987) or Mellor (1998).

$$\frac{\partial \eta}{\partial t}+\frac{\partial UD}{\partial x}+\frac{\partial VD}{\partial y}+\frac{\partial \omega}{\partial \sigma}=0 \quad , \tag{1}$$

$$\frac{\partial UD}{\partial t}+\frac{\partial U^2 D}{\partial x}+\frac{\partial UVD}{\partial y}+\frac{\partial U\omega}{\partial \sigma}-F_x-fVD+gD\frac{\partial \eta}{\partial x}=\frac{\partial}{\partial \sigma}\left[\frac{K_M}{D}\frac{\partial U}{\partial \sigma}\right]+\frac{1}{\rho}\left(\tau_{sx}-\tau_{bx}\right), \tag{2}$$

$$\frac{\partial VD}{\partial t}+\frac{\partial UVD}{\partial x}+\frac{\partial V^2 D}{\partial y}+\frac{\partial V\omega}{\partial \sigma}-F_y+fUD+gD\frac{\partial \eta}{\partial y}=\frac{\partial}{\partial \sigma}\left[\frac{K_M}{D}\frac{\partial V}{\partial \sigma}\right]+\frac{1}{\rho}\left(\tau_{sy}-\tau_{by}\right), \tag{3}$$

$$\frac{\partial q^2 D}{\partial t}+\frac{\partial Uq^2 D}{\partial x}+\frac{\partial Vq^2 D}{\partial y}+\frac{\partial \omega q^2}{\partial \sigma}=\frac{\partial}{\partial \sigma}\left[\frac{K_q}{D}\frac{\partial q^2}{\partial \sigma}\right]+\frac{2K_M}{D}\left[\left(\frac{\partial U}{\partial \sigma}\right)^2+\left(\frac{\partial V}{\partial \sigma}\right)^2\right]-\frac{2Dq^3}{B_1 \ell}+F_q, \tag{4}$$

$$\frac{\partial q^2 \ell D}{\partial t}+\frac{\partial Uq^2 \ell D}{\partial x}+\frac{\partial Vq^2 \ell D}{\partial y}+\frac{\partial \omega q^2 \ell}{\partial \sigma}=\frac{\partial}{\partial \sigma}\left[\frac{K_q}{D}\frac{\partial q^2 \ell}{\partial \sigma}\right]+E_1 \ell \frac{2K_M}{D}\left[\left(\frac{\partial U}{\partial \sigma}\right)^2+\left(\frac{\partial V}{\partial \sigma}\right)^2\right]\tilde{W}-\frac{2Dq^3}{B_1}+F_\ell, \tag{5}$$

where $\sigma = (z-\eta)/(H+\eta)$, H is the mean sea level water depth, U and V are horizontal velocities, $K_M$ and $K_H$ are vertical kinematic viscosity and diffusivity, $K_q$ is vertical turbulence mixing coefficient, $q^2$ is twice the turbulence kinetic energy, $\ell$ is the turbulence length scale, $\tilde{w} = 1+E_2(\ell/kL)$, $k = 0.4$ is the von Karman constant, $L^{-1}=(\eta-z)^{-1}+(H+z)^{-1}$, $B_1$, $E_1$, and $E_2$ are constants, $\tau_s$ and $\tau_b$ are wind stress and bottom friction, $D=H+\eta$ is the total water depth, g is the acceleration due to gravity, f is the Coriolis parameter, $\rho$ is the water density, and $\omega$ is the transformed vertical velocity normal to a sigma surface. The relationship of $\omega$ with Cartesian vertical velocity w is

$$W=\omega+U\left[\sigma\frac{\partial D}{\partial x}+\frac{\partial \eta}{\partial x}\right]+V\left[\sigma\frac{\partial D}{\partial y}+\frac{\partial \eta}{\partial y}\right]+\sigma\frac{\partial D}{\partial t}+\frac{\partial \eta}{\partial t}. \tag{6}$$

And the horizontal viscosity and diffusion terms $F_x$ and $F_y$ are defined as

$$F_x=\frac{\partial}{\partial x}\left[2HA_M\frac{\partial U}{\partial x}\right]+\frac{\partial}{\partial y}\left[HA_M\left(\frac{\partial U}{\partial y}+\frac{\partial V}{\partial x}\right)\right] \tag{7}$$

$$F_y = \frac{\partial}{\partial y}\left[2HA_M \frac{\partial V}{\partial y}\right] + \frac{\partial}{\partial x}\left[HA_M\left(\frac{\partial U}{\partial y} + \frac{\partial V}{\partial x}\right)\right], \tag{8}$$

where $A_M$, the vertically integrated horizontal eddy viscosity, is defined by the Smagorinsky formula

$$A_M = C\Delta x\Delta y\frac{1}{2}\left|\nabla V + (\nabla V)^T\right|, \tag{9}$$

where C, a non-dimensional parameter, is set to be 0.2 in this study; u, $\Delta$x and v, $\Delta$y are the vertically-integrated velocities and grid spacings in the x and y directions for each grid cell;

$$\left|\nabla V + (\nabla V)^T\right|/2 = \left[\left(\frac{\partial u}{\partial x}\right)^2 + \left(\frac{\partial v}{\partial x} + \frac{\partial u}{\partial y}\right)^2/2 + \left(\frac{\partial v}{\partial y}\right)^2\right]^{1/2}. \tag{10}$$

The vertical boundary conditions for (1), (2), and (3) are

$$\omega(0) = \omega(-1) = 0\ , \tag{11}$$

$$\frac{K_M}{D}\left[\frac{\partial U}{\partial \sigma}, \frac{\partial V}{\partial \sigma}\right] = C_z\left[U^2 + V_2\right]^{1/2}(U, V), \sigma \to -1\ , \tag{12}$$

where

$$C_z = MAX\left[\frac{k^2}{\left[\ln\left\{\left(1 + \sigma_{kb-1}\right)H / z_0\right\}\right]^2}, 0.0025\right]\ , \tag{13}$$

$k = 0.4$ is the von Karman constant, $z_0$ is the roughness parameter, and kb is the bottom layer. The boundary conditions for the turbulence closure equations (4) and (5) are

$$\left(q^2(0), q^2\ell(0)\right) = \left(B_1^{2/3}u_\tau^2(0), 0\right), \tag{14}$$

$$\left(q^2(-1), q^2\ell(-1)\right) = \left(B_1^{2/3}u_\tau^2(-1), 0\right), \tag{15}$$

where $B_1$ is one of the turbulence closure constants and $u_\tau$ is the friction velocity at the top or bottom as denoted.

## 2.2. Split Mode

For computational economy, the split mode is used in the model in which the vertically integrated equations (external model) are separated out to calculate the free surface elevation (due to fast moving external gravity waves) from the vertical structure equations, where the vertical velocity shear (slow moving internal gravity waves) are calculated.

## 2.3. Time Step Constraints

The external mode of the model time step is limited by the Courant-Friedrichs-Levy (CFL) computational stability condition

$$\Delta t_E \leq \frac{1}{C_t}\left|\frac{1}{\Delta x^2}+\frac{1}{\Delta y^2}\right|^{-1/2} \tag{16}$$

where $C_t = 2(gH)^{1/2} + U_{max}$; $U_{max}$ is the expected maximum velocity. The internal mode time step ($\Delta t_I$) criteria is analogous to, however much less stringent than, that for the external model. Typical ratio of the time steps, $\Delta t_I/\Delta t_E$, for an estuarine is on the order of 10.

## 2.4. Model Grid

A coarse model grid has been constructed to cover the New York Harbor and vicinity estuarines from 74° 10' W to 73° 45' W and from 40° 24' N to 40° 52' N including the East River, Hudson River up to Poughkeepsie, the Newark Bay, the Hackensack and Passic Rivers, Arthur Kill, the Raritan River, and Raritan Bay (Figure 2.1). The grid itself is orthogonal and is sufficiently fine to minimize truncation errors. The horizontal resolution varies spatially and ranges from 150 to 1000 m, resulting in 134 by 73 grid points in the cross- and along- harbor direction. The model water depth ranges from 3 m in the shallow shoals to 25 m in the navigation channel near The Narrows (Figure 2.2). The Hudson River north of Spuyten Duyvil has been "bent" to take into account the river effect and to save on computational cost.

A fine grid, dimensioned 126 by 38 (shaded area in Figure 2.1 and Figure 2.3) and covering the critical navigation waterways of Kill van Kull and Newark Bay, has been developed and embedded within the original (coarse) grid. The grid resolution for the nested grid is double that of the coarse grid. The fine grid takes hydrodynamic information at the interface between the coarse and fine grids. Due to the a higher spatial resolution, the fine grid is then capable of resolving small scale eddies in more detail.

Although the New York Harbor is hydrodynamically connected with Long Island Sound and the NY Bight, for the operational nowcast/forecast model system to fully utilize information from NOS's Physical Oceanographic Real Time System (PORTS) as lateral boundary conditions, the model grid open boundary has been set at Willets Point, New York, and Sandy Hook, New Jersey.

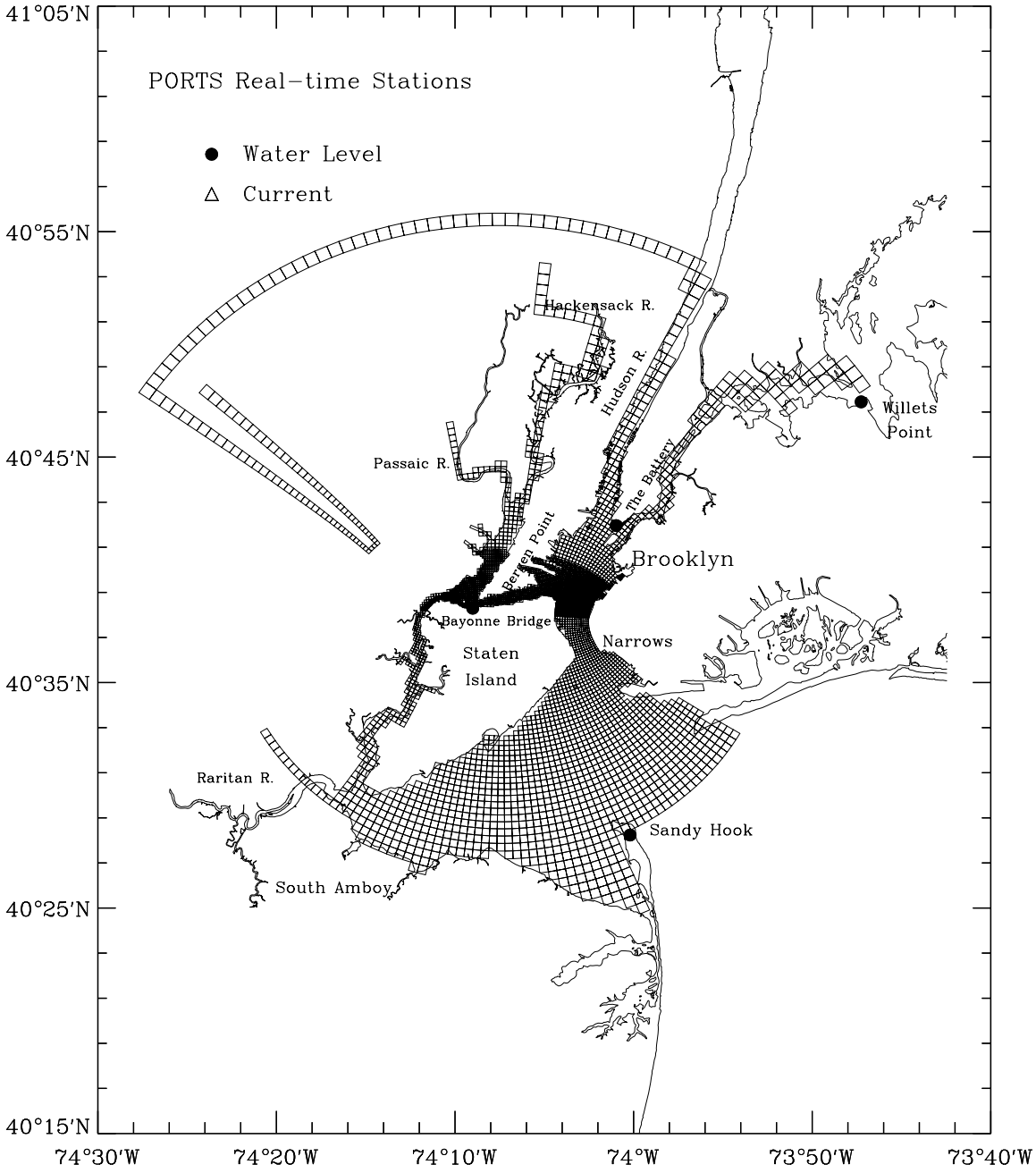


**Figure 2.1.** New York/New Jersey Harbor model grid showing locations of water level gages and current meter.

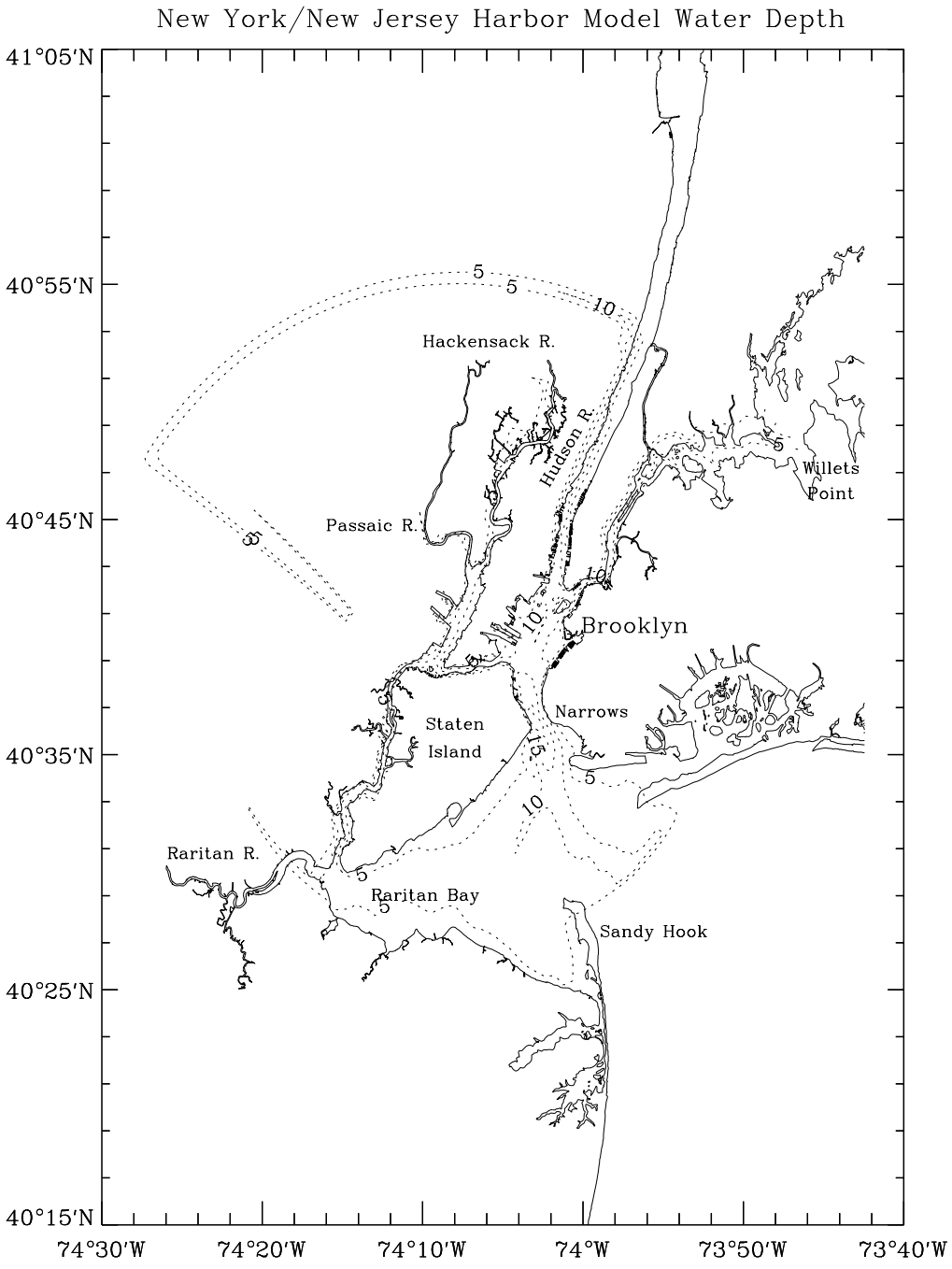


**Figure 2.2.** New York/New Jersey Harbor model bathymetry, contours in meter.

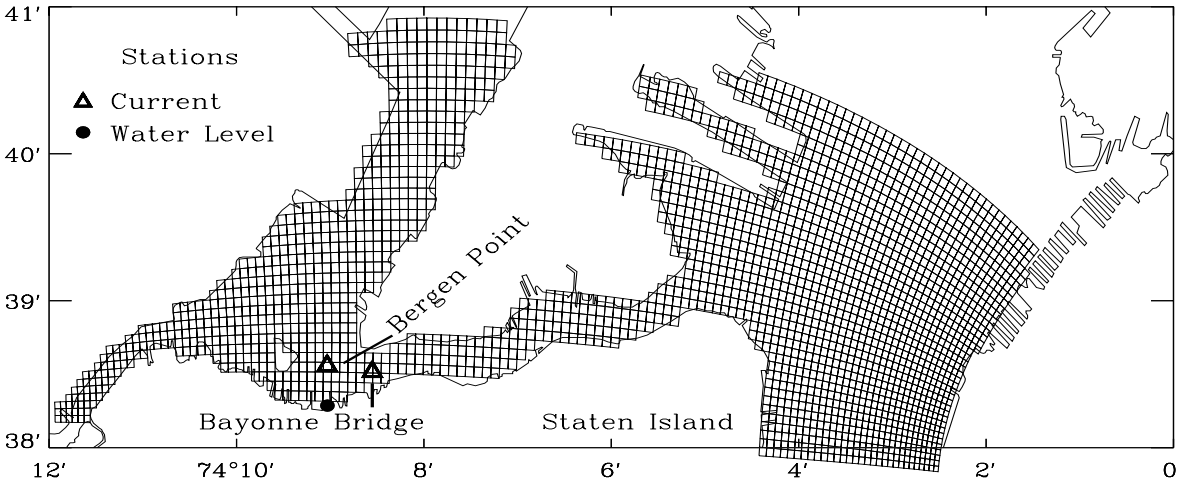


**Figure 2.3.** Nested fine grid.

## 3. MODEL COUPLING

The curvilinear coordinate system used in the model allows fine grids in regions near the Narrows and the navigation channel approaching Kill Van Kull and Port Elizabeth. This gives us the ability to provide detailed water level and current information where water currents change dramatically, however, the placement of the fine grid is constrained by the orthogonality requirement. This means that refined grid resolution in one part of the model region is often done at the expense of grid resolution in other subregions. Thus the choice of where in the modeled coastal ocean one can put more grid points is not completely arbitrary. The information given by the coarse model is not able to satisfy mariners and Coast Guard requirements for the purposes of safe navigation, efficient oil-spill cleanup and managing vessel traffic, especially for the region of the tidal eddy in the west entrance of the Kill Van Kull, which was confirmed by a towed ADCP survey conducted in 1993 (Parker, 1996). In order to provide more accurate detailed current information in these areas, a fine grid (FG) model has been developed and nested in the coarse grid (CG). The spatial resolution of the fine grid is twice that of the coarse grid. There are 7 sigma levels in the vertical in both the CG and the FG, although extension to cases with different sigma levels is conceptually not difficult but does require extensive coding. There are two coupling methods that exchange fluxes across the grid interface (Oey and Chen, 1992) : one-way and two-way couplings. In the one-way coupling, the FG is driven by fluxes from the CG through the grid interface, and the FG does not feedback any information to the CG. In the two-way coupling, in addition to providing open boundary conditions for FG model, CG model also receives flux feedback information from FG model. For convenience, the model is coded such that a common block was set up to communicate field variables at interface between two model grids. Both the CG and the FG models are independent and compiled separately before being coupled, however, the two models run in parallel. At present, the model uses the one-way coupling approach in which the FG model obtains the water elevations and fluxes from the CG model through the common block.

The evaluation of one- and two- way coupling results is summarized in Chapter 4, Model Hindcasts.

### 3.1. Grid Comparison

Key features of the two model grids are listed below for comparison:

(1) Coarse Grid
Dimension : 73x134x7
Horizontal Resolution: from 170 to 1000 m
Nested Area: I, from 7 to 71
J, from 65 to 85

(2) Fine Grid
Dimension : 26x38x7
Horizontal Resolution: from 70 to 150 m, half of the corresponding coarse grid cell.

(3) Vertical Structure:
The CG and nested FG have same number of vertical sigma levels.
$K_{coarse\text{-}grid}=K_{fine\text{-}grid}=7$

(4) Grid Generation
The FG coordinates are interpolated from the CG with half of the corresponding CG cell size.

(5) Water Depth Setup
The FG water depths are bilinearly interpolated from the FG.

(6) Nested Grid Model Initialization
The FG is initialized with parameters (velocity flux and water level) interpolated from the CG when the FG model starts.

(7) Interaction Between CG and FG
Set up a common block between the CG model and FG model so that the two models can only interact with each other through this common block. Thus, the parameter name remains the same in the same function subroutines of two models.

(8) Time stepping
The CG model's external time step is N times the FG model's external time step, while the two models have the same internal time step.

(9) Boundary Forcing
The boundary conditions in the FG are interpolated from their overlapped CG cells at each external time step.

(10) Model Spin-up
The CG model starts first and the FG model can start at any time once the CG model is started.

## 3.2. Coupling Considerations

Many factors such as model physics, grid interaction, conservation properties, computational expense and model applications are taken into account to design a nested model.

### 3.2.1. Interface Conditions

The interface conditions are designed to maintain continuity and compatibility of solutions between the two model grids. Following computation of variables in the CG model domain, all flux and field variables at the input dynamic interface are saved and then interpolated along input interfaces as the FG model boundary solution. Because of the nature of the staggered grid, the spatial relationships between CG model and FG model points are different for the flux and field variables. It is important

to point out that the flux and the mass at the interface between the CG model and FG model must be conserved.

In the two-way coupling, the feedback from the FG model to CG model is obtained at every second time step of the FG model (i.e., when both FG model and CG model are at the same time level) by satisfying the flux conservation at the feedback dynamic interface, where a CG model flux location coincides with corresponding FG model flux locations. All other field variables are obtained from this specification.

The preceding specification of interface conditions allows two-way interaction of physical processes to be accomplished. The CG model system provides the FG model with the larger scale forcing through the dynamic interface and then the FG model affects the larger scale through the feedback interface. However, it is noted that the FG model values at the boundary are specified externally from the CG model values and do generate some numerical noise. Therefore, values at points next to the FG model boundary must not be included in the feedback process. On the other hand, it is better to place the feedback interface as close as possible to the dynamic interface in order to maximize the use of information about the FG model variables in the CG model solution (see Section 3.4 for detail formulation and schematic representation).

### 3.2.2. Noise Control

Most nested grid models exhibit a compatibility problem at the interface where the two grid systems meet due to the nonuniform nature of the grids. For instance, a disturbance propagating from the CG model to the FG model may induce false reflection back to the CG model and scattering into the FG model. Likewise, a disturbance propagating from the FG model to the CG model may also experience false reflection back onto the FG model. These interface generated problems may lead to numerical instabilities that can seriously affect the simulated results over the entire domain. This is known as the interface condition problem. As Zhang and Chang (1986) pointed out, an optimal interface procedure which has the following two properties could eliminate this problem: 1) all resolvable waves propagate across the interface smoothly with only minimal changes in amplitude and minimum reflection of energy, and 2) mass, momentum and total energy exchanged between the two grid systems are conserved.

To satisfy the first condition, which is important to allow the nested grid system to operate effectively, special noise control techniques must be used. Many methods have been employed for two-way nesting system. Jones (1977) found that the spatial smoother is the most effective method of noise control compared to other methods tested. In our model, a flow relaxation scheme, similar to that of Oey and Chen (1992), is applied to the dynamic interface and feedback interface between FG model and CG model. For the x component depth-averaged velocity, for example, that is

$$U_C = aU_F + (1-a)U_C \quad (17)$$

where the subscript F denotes the values interpolated from the FG model to the corresponding CG model, the subscript C indicates the values from the CG model, and a is the weight parameter (ranges from zero at FG model feedback row to 1 at the two grid systems interface).

For the second condition, the exact conservation of momentum flux at the interface of two grid systems is satisfied in our model.

### 3.2.3. Initialization

It is highly desirable that the initial conditions of the FG model and the CG model be determined in such a way that the fields in the overlap region are compatible when the integration begins. The procedure for obtaining the grid points values starts with the CG model and then interpolated to the FG model corresponding points by a bilinear interpolation. These data include flux and three-dimensional field variables. In order to attain better quality interface conditions, the bathymetry between the dynamic interface and feedback interface are specified as the same. So both the FG model and CG model will have the same variable in this area.

### 3.2.4. Programing Considerations

In constructing the nested New York/New Jersey model, the interface between the CG model and FG model has been placed parallel to the CG model axis. When the CG information and its field variables and the FG information are given, all the necessary information for the FG model integration such as surface forcing, and field variables, are automatically generated by bilinear interpolation. The information over the interface zone shared by the FG model and CG model are stored in the special common blocks, thus minimizing coding errors and simplifying the coupling procedure coding.

## 3.3. Coupling Procedures

Figure 3.1 shows a schematic diagram illustrating the procedure of a typical barotropic POM run without coupling. With the nested grid one-way coupled, the diagram is shown as in Figure 3.2 where the right side is the FG model procedure. The process underlined in Figure 3.3 indicates the two-way coupling procedure, in addition to the one-way coupling procedure.

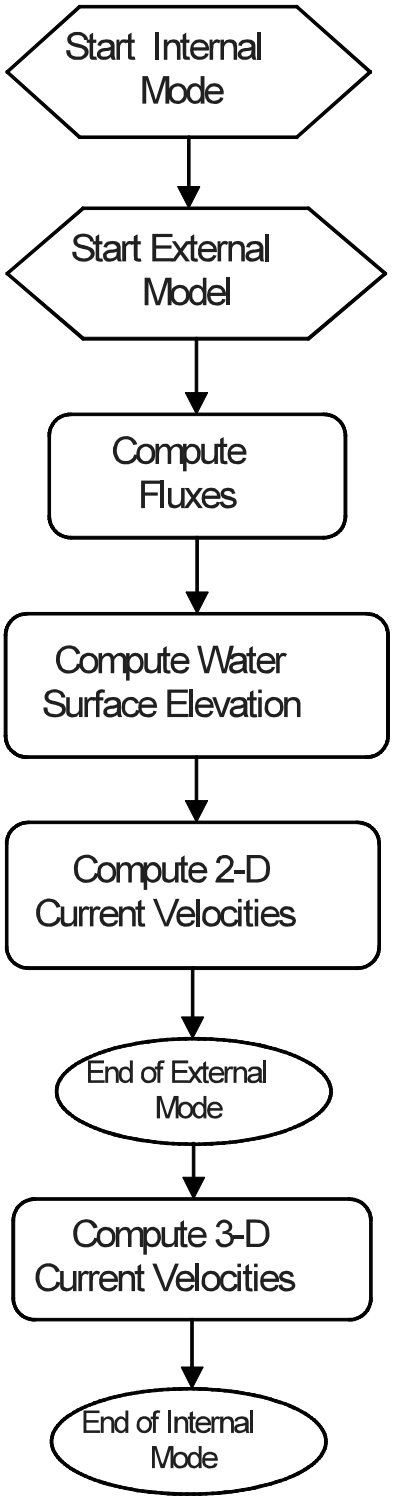


**Figure 3.1.** Schematic diagram for an uncoupled three-dimensional barotropic POM.

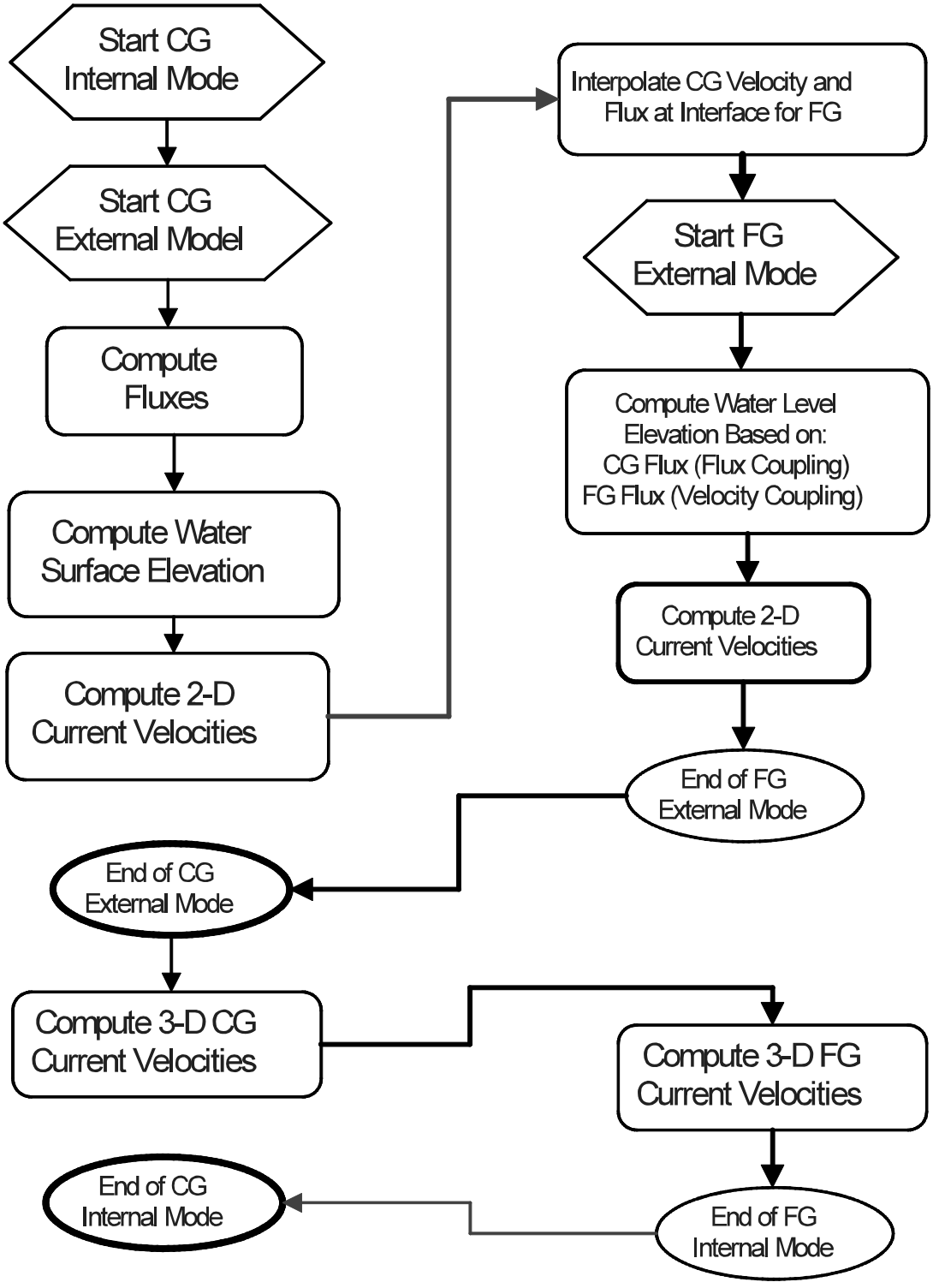


**Figure 3.2.** Schematic diagram for a one-way coupled 3-dimensional barotropic POM.

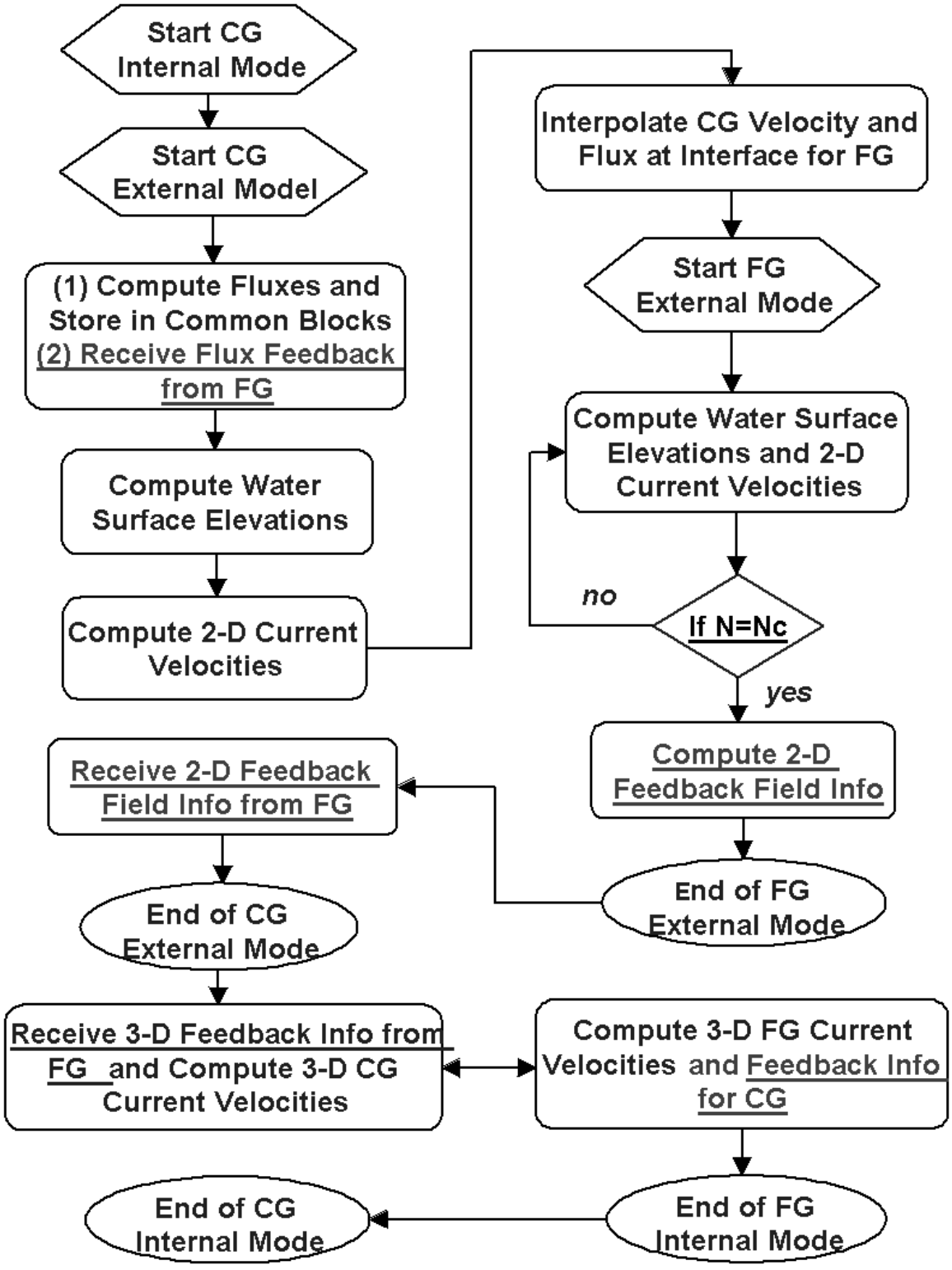


**Figure 3.3.** Schematic diagram for a two-way coupled 3-dimensional barotropic POM.

### 3.4. Two-Way Coupling Finite Difference Equations

The one-way coupling algorithm is simple and straight forward for computer program coding. Here the finite difference form of the feedback from the FG model to CG model for the two-way coupling at the southern and northern boundary interface (east and west can be derived following similar notation) are listed as follows. Figure 3.4 illustrates the schematic representation of the nested grid coupling.

The following are the equations at the southern boundary:

$$Vflux(ic,jc)=Vflux(in,jn)+Vflux(in+1,jn),$$

$$V(ic,jc)=(av\overline{H(in,jn)}V(in,jn)+(1-av)\overline{H(in+1,jn)}V(in+1,jn))/\overline{H(ic,jc)},$$

where

$$\overline{H(ic,jc)}=(H(ic,jc)+H(ic,jc-1))/2,$$

$$\overline{H(in,jn)}=(H(in,jn)+H(in,jn-1))/2,$$

$$av=\frac{\overline{\Delta x(in,jn)}}{\overline{\Delta x(ic,jc)}}=\frac{\Delta x(in,jn)+\Delta x(in,jn-1)}{\Delta x(ic,jc)+\Delta x(ic,jc-1)},$$

$$\eta(ic,jc-1)=\eta(in,jn-2)S(in,jn-2)+\eta(in+1,jn-2)S(in+1,jn-2)+$$
$$\eta(in+1),jn-1)S(in+1,jn-1)+\eta(in,jn-1)S(in,jn-1))/S(ic,jc-1),$$

$$U(ic,jc+1)==(U(in,jn-1)\Delta y(in,jn-1)+U(in,jn-2)\Delta y(in,jn-2))/\Delta y(ic,jc+1),$$

or

$$U(ic,jc+1)=(au\overline{H(in,jn-2)}U(in,jn-2)+(1-au)\overline{H(in+1,jn-1)}U(in,jn-1))/\overline{H(ic,jc+1)},$$

where

$$\overline{H(ic,jc+1)}=(H(ic-1,jc+1)+H(ic,jc+1))/2,$$

$$\overline{H(in,jn-2)}=(H(in-1,jn-2)+H(in,jn-2))/2,$$

$$au=\frac{\overline{\Delta y(in,jn-2)}}{\overline{\Delta y(ic,jc+1)}}=\frac{\Delta y(in,jn-2)+\Delta y(in-1,jn-2)}{\Delta y(ic,jc+1)+\Delta y(ic-1,jc+1)},$$

$$\ldots\ldots\ i_c=il,\ ir;\ j_c=jb+1;\ i_n=3,\ IMn-2;\ j_n=3$$

where subscripts c and n denote coarse and fine grids, au and av are the weigh parameter for U and V, il and ir are interface i-index of CG model, S is the surface area (equivalent to art(ic,jc) for coarse grid and art(in,jn) for fine grid), IMn and JMn are the dimensions of the FG model.

The following are the equations at the northern boundary:

$$Vflux(ic,jc)=Vflux(in,jn)+Vflux(in+1,jn),$$

$$V(ic,jc)=(av\overline{H(in,jn)}V(in,jn)+(1-av)\overline{H(in+1,jn)}V(in+1,jn))/\overline{H(ic,jc)},$$

where

$$\overline{H(ic,jc)}=(H(ic,jc)+H(ic,jc-1))/2,$$

$$\overline{H(in,jn)}=(H(in,jn)+H(in,jn-1))/2,$$

$$av=\frac{\overline{\Delta x(in,jn)}}{\overline{\Delta x(ic,jc)}}=\frac{\Delta x(in,jn)+\Delta x(in,jn-1)}{\Delta x(ic,jc)+\Delta x(ic,jc-1)},$$

$$\eta(ic,jc-1)=\eta(in,jn-2)S(in,jn-2)+\eta(in+1,jn-2)S(in+1,jn-2)+$$
$$\eta(in+1),jn-1)S(in+1,jn-1)+\eta(in,jn-1)S(in,jn-1))/S(ic,jc-1),$$

$$U(ic,jc-1)==(U(in,jn-1)\Delta y(in,jn-1)+U(in,jn-2)\Delta y(in,jn-2))/\Delta y(ic,jc-1),$$

or

$$U(ic,jc-1)=(au\overline{H(in,jn-2)}U(in,jn-2)+(1-au)\overline{H(in+1,jn-1)}U(in,jn-1))/\overline{H(ic,jc-1)},$$

where

$$\overline{H(ic,jc-1)}=(H(ic-1,jc-1)+H(ic,jc-1))/2,$$

$$\overline{H(in,jn-2)}=(H(in-1,jn-2)+H(in,jn-2))/2,$$

$$au=\frac{\overline{\Delta y(in,jn-2)}}{\overline{\Delta y(ic,jc-1)}}=\frac{\Delta y(in,jn-2)+\Delta y(in-1,jn-2)}{\Delta y(ic,jc-1)+\Delta y(ic-1,jc-1)},$$

..... $ic=il,\ ir;\ jc=jt-1;\ in=3,\ IMn-2;\ jn=JMn-2$

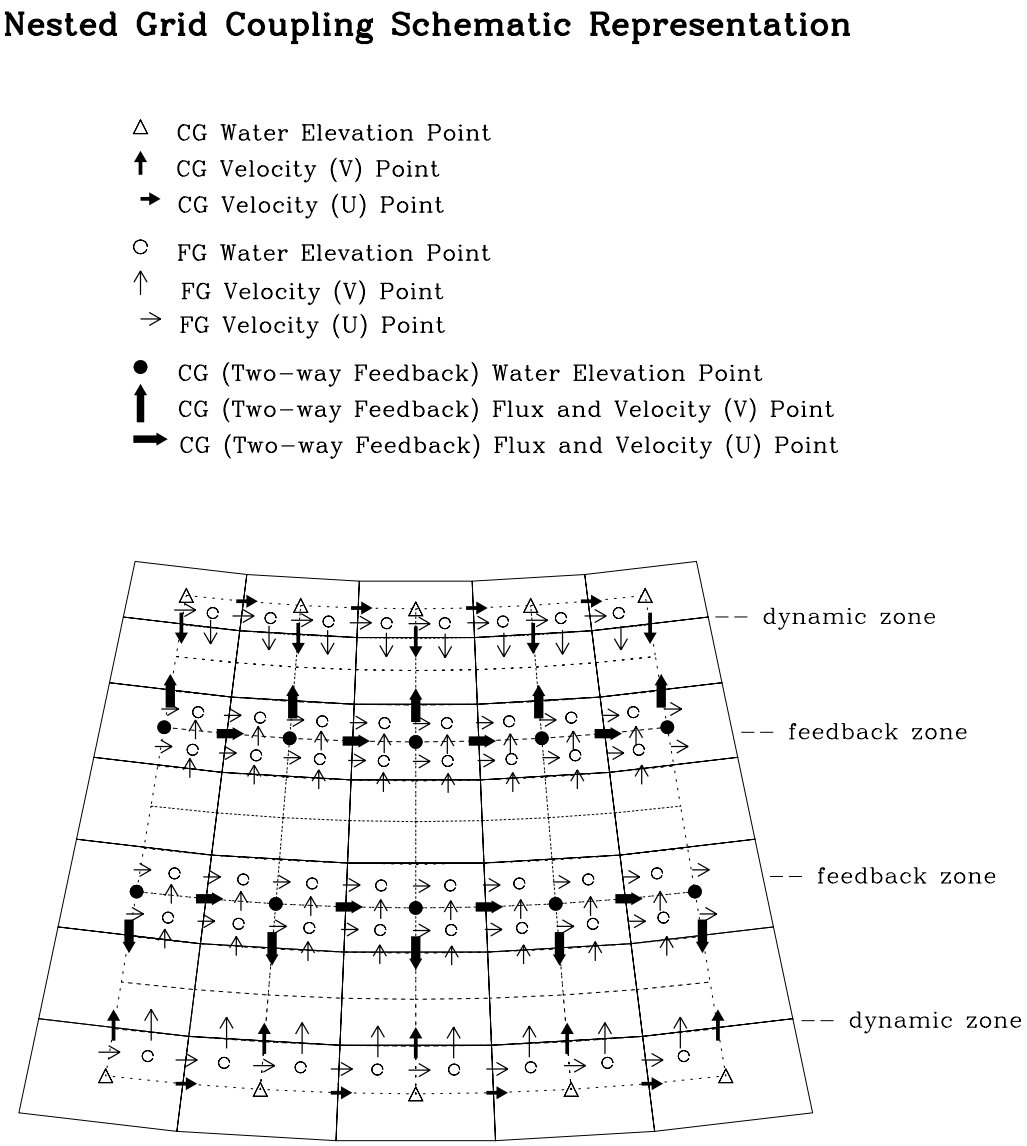


**Figure 3.4.** Nested grid coupling schematic representation.

# 4. TIDE SIMULATIONS

The barotropic three-dimensional barotropic model described in Chapter 2 was calibrated with astronomical tide simulation. NOS accepted harmonic constants (Table 4.1 referenced to UTC) at Sandy Hook and Willets Point were used to generate astronomical tide as open boundary conditions predictions for the year of 1997. Winds, atmospheric pressure, and river discharge were turned off. The internal and external time steps were specified as 12 and 6 seconds, respectively.

After several test simulations, key hydrodynamic parameters are determined based on the comparison between simulated and harmonically generated tides at the Bayonne Bridge and The Battery, the two locations inside the model grid with long term water level records qualified for NOS to provide accepted harmonic constants. Among other parameters, the roughness depth is specified as 0.1 cm and the horizontal diffusivity constant C in Equation 8 as 0.1. Water depth and the land-water boundary are also adjusted, especially along the Kill Van Kull navigational channel, based on the most recent nautical charts and 1996 USACE dredging plan map. The yearly simulation starts on January 1, 1997 after 10 days of spin up. The simulated tide and tidal current at Bayonne Bridge, and tide at The Battery, are saved at 6 minute intervals for analysis. Figure 4.1shows two days of tide predictions and simulated tides from the fine and coarse grids at the Bayonne Bridge and The Battery (see Figure 2.1 for locations), and tidal currents at Bayonne Bridge in layers 2 and 4. Overall, the simulated tidal water levels have a better accuracy than tidal currents and the simulated currents from the fine grid are more accurate than those of the coarse grid.

## 4.1. Water Level

### 4.1.1. Harmonic Constants

The least square program used by the NOS tidal analysis programs (Zervas, 1999), based on Schureman (1971) has been applied to obtain 37 harmonic constants by analyzing 6 minute interval simulated tides at the Bayonne Bridge and The Battery for the entire 1997 year. Tables 4.2 and 4.3 show the comparison of NOS accepted and model simulated amplitude and epoch for each constituent at two locations. It can be seen that $M_2$ is the predominate tide component in New York Harbor. At the Bayonne Bridge, the $M_2$ amplitude and epoch differences between NOS accepted and model values are 1.7 cm and 3.3 degrees, respectively. The values are derived from the embedded fine grid model results. Values derived from the coarse grid model results shows slightly greater errors (4.4 cm and 3.9 degrees) than that from the fine grid, indicating that model accuracy increases slightly with grid resolution. Amplitude and epoch differences appear to be greater at The Battery (5.9 cm and 7.6 degrees for $M_2$). This is probably due to the location of The Battery outside the fine grid domain. Differences for other tide components are insignificant both in amplitude and epoch.

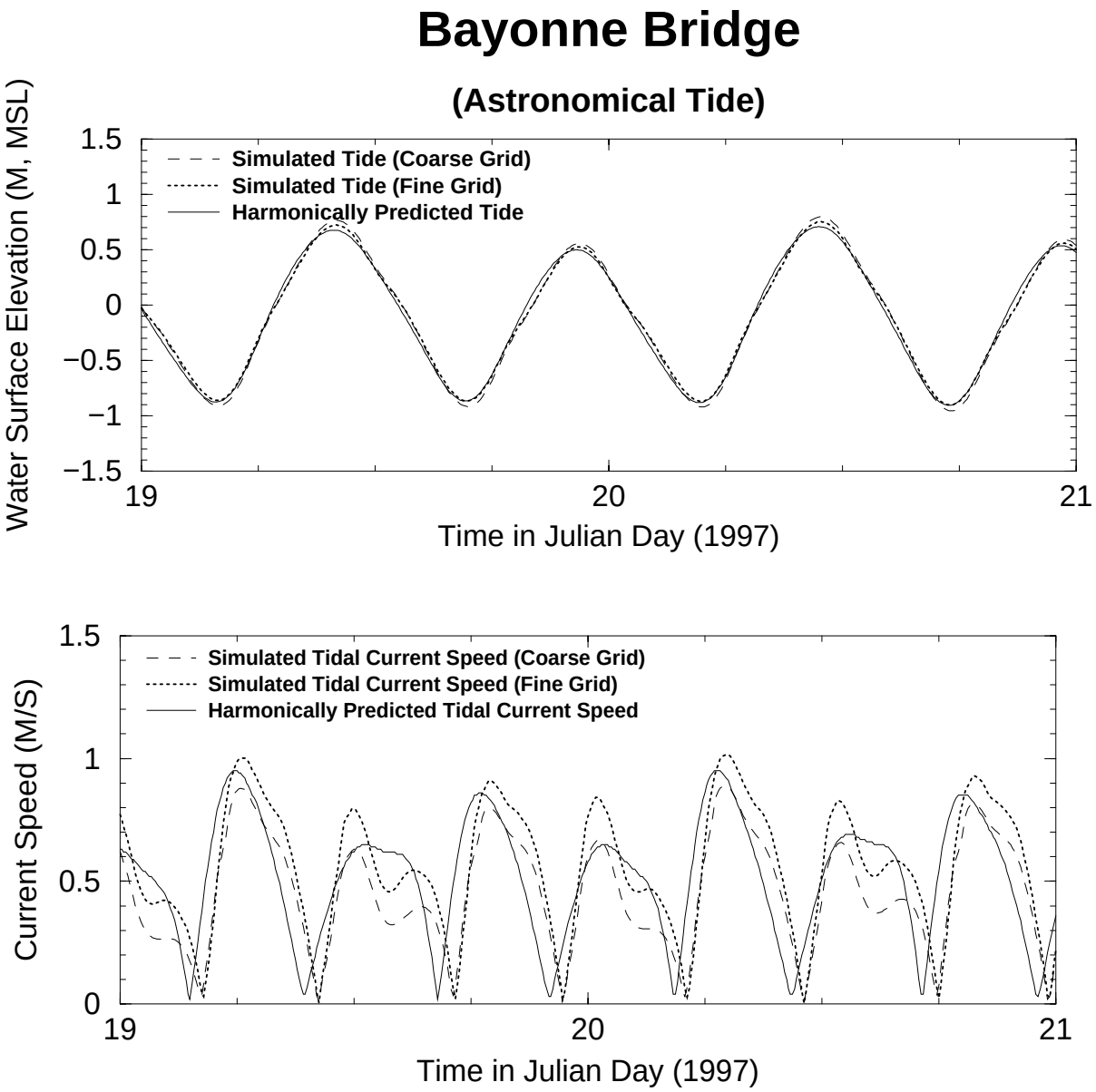


**Figure 4.1.** Harmonically predicted and simulated tide (top) and tidal current (bottom) from fine and coarse grids at Bayonne Bridge.

**Table 4.1.** Harmonic constants at Sandy Hook and Willets Point for yearly tidal simulation.

| | | Sandy Hook | | Willets Point | |
|---|---|---|---|---|---|
| | Name | Amp. (m) | Epoch (degree) | Amp. (m) | Epoch (degree) |
| 1 | M2 | 0.693 | 7.5 | 1.091 | 118.1 |
| 2 | S2 | 0.137 | 35.4 | 0.189 | 144.4 |
| 3 | N2 | 0.157 | 349.7 | 0.240 | 97.9 |
| 4 | K1 | 0.105 | 175.3 | 0.094 | 194.7 |
| 5 | M4 | 0.015 | 266.3 | 0.036 | 152.2 |
| 6 | O1 | 0.054 | 171.2 | 0.065 | 221.5 |
| 7 | M6 | 0.017 | 90.7 | 0.076 | 166.4 |
| 8 | MK3 | 0.005 | 57.9 | 0.010 | 208.7 |
| 9 | S4 | 0.010 | 14.0 | 0.000 | 0.0 |
| 10 | MN4 | 0.007 | 276.0 | 0.022 | 126.2 |
| 11 | NU2 | 0.030 | 349.9 | 0.054 | 96.3 |
| 12 | S6 | 0.000 | 0.0 | 0.000 | 0.0 |
| 13 | MU2 | 0.026 | 14.9 | 0.000 | 0.0 |
| 14 | 2N2 | 0.022 | 333.0 | 0.024 | 81.3 |
| 15 | OO1 | 0.004 | 203.6 | 0.000 | 0.0 |
| 16 | LAM2 | 0.009 | 356.1 | 0.021 | 138.9 |
| 17 | S1 | 0.010 | 136.9 | 0.000 | 0.0 |
| 18 | M1 | 0.004 | 173.2 | 0.009 | 225.5 |
| 19 | J1 | 0.004 | 177.4 | 0.005 | 181.2 |
| 20 | MM | 0.000 | 0.0 | 0.039 | 233.8 |
| 21 | SSA | 0.030 | 56.1 | 0.027 | 42.3 |
| 22 | SA | 0.064 | 126.5 | 0.060 | 135.7 |
| 23 | MSF | 0.000 | 0.0 | 0.020 | 215.9 |
| 24 | MF | 0.000 | 0.0 | 0.018 | 268.7 |
| 25 | RHO | 0.002 | 169.3 | 0.000 | 0.0 |
| 26 | Q1 | 0.010 | 177.4 | 0.014 | 202.5 |
| 27 | T2 | 0.011 | 16.4 | 0.011 | 144.3 |
| 28 | R2 | 0.001 | 36.5 | 0.000 | 0.0 |
| 29 | 2Q1 | 0.001 | 167.0 | 0.000 | 0.0 |
| 30 | P1 | 0.032 | 175.5 | 0.032 | 206.1 |
| 31 | 2SM2 | 0.000 | 0.0 | 0.000 | 0.0 |
| 32 | M3 | 0.011 | 61.2 | 0.000 | 0.0 |
| 33 | L2 | 0.028 | 9.1 | 0.092 | 136.3 |
| 34 | 2MK3 | 0.007 | 37.2 | 0.009 | 193.5 |
| 35 | K2 | 0.036 | 35.1 | 0.051 | 141.9 |
| 36 | M8 | 0.000 | 0.0 | 0.000 | 0.0 |
| 37 | MS4 | 0.011 | 235.4 | 0.009 | 174.1 |

**Table 4.2.** Comparison of modeled and NOS accepted harmonic constants at Bayonne Bridge.

| | | NOS | | Model | |
|---|---|---|---|---|---|
| | | Amp. (m) | Epoch (degree) | Amp. (m) | Epoch (degree) |
| 1 | M2 | 0.745 | 21.2 | 0.728 | 24.5 |
| 2 | S2 | 0.143 | 51.3 | 0.142 | 54.8 |
| 3 | N2 | 0.166 | 5.1 | 0.161 | 7.6 |
| 4 | K1 | 0.106 | 182.9 | 0.103 | 182.2 |
| 5 | M4 | 0.036 | 292.4 | 0.028 | 324.9 |
| 6 | O1 | 0.053 | 179.3 | 0.052 | 177.7 |
| 7 | M6 | 0.021 | 174.3 | 0.029 | 140.8 |
| 8 | MK3 | 0.010 | 72.8 | 0.007 | 99.9 |
| 9 | S4 | 0.014 | 44.5 | 0.012 | 57.5 |
| 10 | MN4 | 0.017 | 291.5 | 0.012 | 319.4 |
| 11 | NU2 | 0.034 | 1.6 | 0.031 | 6.9 |
| 12 | S6 | 0.000 | 0.0 | 0.000 | 0.0 |
| 13 | MU2 | 0.029 | 38.1 | 0.027 | 41.3 |
| 14 | 2N2 | 0.021 | 345.0 | 0.022 | 354.7 |
| 15 | OO1 | 0.003 | 204.5 | 0.004 | 221.5 |
| 16 | LAM2 | 0.013 | 2.3 | 0.012 | 7.8 |
| 17 | S1 | 0.013 | 139.7 | 0.010 | 143.7 |
| 18 | M1 | 0.007 | 245.9 | 0.004 | 182.7 |
| 19 | J1 | 0.005 | 204.0 | 0.003 | 195.4 |
| 20 | MM | 0.000 | 0.0 | 0.005 | 204.3 |
| 21 | SSA | 0.031 | 58.4 | 0.029 | 56.7 |
| 22 | SA | 0.074 | 129.2 | 0.061 | 127.2 |
| 23 | MSF | 0.000 | 0.0 | 0.005 | 199.5 |
| 24 | MF | 0.000 | 0.0 | 0.002 | 219.7 |
| 25 | RHO | 0.003 | 181.5 | 0.002 | 175.7 |
| 26 | Q1 | 0.011 | 191.3 | 0.009 | 185.9 |
| 27 | T2 | 0.013 | 30.4 | 0.012 | 34.7 |
| 28 | R2 | 0.005 | 270.2 | 0.001 | 60.4 |
| 29 | 2Q1 | 0.001 | 175.7 | 0.000 | 0.0 |
| 30 | P1 | 0.033 | 181.8 | 0.031 | 183.4 |
| 31 | 2SM2 | 0.000 | 0.0 | 0.002 | 225.1 |
| 32 | M3 | 0.012 | 86.6 | 0.013 | 90.3 |
| 33 | L2 | 0.026 | 10.2 | 0.032 | 25.1 |
| 34 | 2MK3 | 0.009 | 46.1 | 0.010 | 58.4 |
| 35 | K2 | 0.040 | 47.9 | 0.037 | 54.8 |
| 36 | M8 | 0.000 | 0.0 | 0.006 | 106.4 |
| 37 | MS4 | 0.018 | 284.9 | 0.012 | 290.1 |

**Table 4.3.** Comparison of modeled and NOS accepted harmonic constants at The Battery.

| | | NOS | | Model | |
|---|---|---|---|---|---|
| | | Amp. (m) | Epoch (degree) | Amp. (m) | Epoch (degree) |
| 1 | M2 | 0.671 | 19.4 | 0.730 | 27.0 |
| 2 | S2 | 0.133 | 45.3 | 0.141 | 55.0 |
| 3 | N2 | 0.149 | 0.9 | 0.162 | 9.0 |
| 4 | K1 | 0.102 | 180.4 | 0.107 | 181.5 |
| 5 | M4 | 0.025 | 252.3 | 0.022 | 252.8 |
| 6 | O1 | 0.054 | 177.1 | 0.056 | 179.0 |
| 7 | M6 | 0.028 | 153.1 | 0.030 | 154.3 |
| 8 | MK3 | 0.009 | 85.1 | 0.006 | 83.1 |
| 9 | S4 | 0.012 | 17.4 | 0.012 | 46.1 |
| 10 | MN4 | 0.010 | 263.9 | 0.006 | 258.6 |
| 11 | NU2 | 0.028 | 0.8 | 0.032 | 10.8 |
| 12 | S6 | 0.000 | 0.0 | 0.000 | 0.0 |
| 13 | MU2 | 0.025 | 9.2 | 0.024 | 30.9 |
| 14 | 2N2 | 0.018 | 346.2 | 0.022 | 352.1 |
| 15 | OO1 | 0.002 | 183.6 | 0.004 | 218.9 |
| 16 | LAM2 | 0.011 | 19.4 | 0.010 | 17.7 |
| 17 | S1 | 0.012 | 133.8 | 0.010 | 143.1 |
| 18 | M1 | 0.004 | 178.7 | 0.004 | 181.9 |
| 19 | J1 | 0.004 | 182.0 | 0.004 | 190.9 |
| 20 | MM | 0.000 | 0.0 | 0.004 | 212.2 |
| 21 | SSA | 0.030 | 54.6 | 0.030 | 55.7 |
| 22 | SA | 0.077 | 131.8 | 0.063 | 126.8 |
| 23 | MSF | 0.000 | 0.0 | 0.003 | 207.5 |
| 24 | MF | 0.000 | 0.0 | 0.002 | 257.6 |
| 25 | RHO | 0.002 | 175.7 | 0.002 | 174.0 |
| 26 | Q1 | 0.012 | 189.8 | 0.010 | 185.0 |
| 27 | T2 | 0.011 | 28.2 | 0.011 | 34.4 |
| 28 | R2 | 0.001 | 45.3 | 0.000 | 0.0 |
| 29 | 2Q1 | 0.002 | 173.7 | 0.001 | 169.6 |
| 30 | P1 | 0.031 | 182.2 | 0.033 | 183.0 |
| 31 | 2SM2 | 0.000 | 0.0 | 0.001 | 224.0 |
| 32 | M3 | 0.010 | 81.4 | 0.012 | 85.2 |
| 33 | L2 | 0.015 | 21.6 | 0.031 | 39.8 |
| 34 | 2MK3 | 0.006 | 61.1 | 0.008 | 58.4 |
| 35 | K2 | 0.036 | 44.0 | 0.037 | 54.8 |
| 36 | M8 | 0.004 | 329.7 | 0.002 | 29.4 |
| 37 | MS4 | 0.016 | 250.8 | 0.017 | 261.2 |

### 4.1.2. Skill Assessment for Tidal Level

A standard suit of assessment statistics is defined in NOS (1999). Parameters in the suite calculated based on the time series of harmonically predicted and model simulated tidal water levels (hourly) at the Bayonne Bridge and The Battery are derived. Defining the error as the predicted tide minus the simulated tide, these parameters are (NOS, 1999):

1. SM: Series mean.
2. SD: Standard deviation of the error.
1. RMSE: Root mean squared error.
2. CF(x): Central Frequency. Percentage of errors that lie within the limit ±x
3. POF(x): Positive Outlier Frequency. Percentage of errors that are greater than x.
4. NOF(x): Negative Outlier Frequency. Percentage of errors that are less than x.
5. MDPO(x): Maximum Duration of Positive Outliers. A positive outlier event is two or more consecutive occurrences of an error greater than x. MDPO is the length (number of consecutive occurrences) of the longest event.
6. MDNO(x): Maximum Duration of Negative Outliers. A negative outlier event is two or more consecutive occurrences of an error less than -x. MDNO is the length (number of consecutive occurrences) of the longest event.

Table 4.4 lists these parameters at Bayonne Bridge and The Battery. The criteria accepted by NOS are also included in the table. All model statistical parameters pass the criteria.

**Table 4.4.** Tide simulation water level skill assessment standard statistics for entire time series at Bayonne Bridge and The Battery.

| | Bayonne Bridge | | | The Battery | | | NOS Accepted Criteria |
|---|---|---|---|---|---|---|---|
| | Predicted | Model | Difference | Predicted | Model | Difference | |
| SM (cm) | 0.04 | -1.43 | -1.47 | 0.04 | -2.53 | -2.56 | na |
| SD (cm) | na | na | 4.68 | na | na | 8.87 | na |
| RMSE (cm) | na | na | 4.91 | na | na | 9.23 | na |
| CF (15 cm) % | 99.1 | | | 92.1 | | | ≥ 90 |
| POF (30 cm) % | 0 | | | 0 | | | ≤1 |
| NOF (30 cm) % | 0 | | | 0 | | | ≤1 |
| MDPO (30 cm) (Hour) | 0 | | | 0 | | | ≤ 24 |
| MDNO (30 cm) (Hour) | 0 | | | 0 | | | ≤ 24 |

### 4.1.3. Skill Assessment for High and Low Tidal Level

A standard suit of assessment statistics for the amplitude and time at high and low water time series is computed. This subset time series for high and low water is derived from the entire 6 minute interval model simulated and harmonically predicted tide time series. Differences of amplitude and time between the subset time series are computed and the standard suit of statistical parameters are derived and listed in Tables 4.5 and 4.6. All model parameters pass the criteria.

**Table 4.5.** Tide simulation high and low water level skill assessment standard statistics at Bayonne Bridge.

| | Bayonne Bridge | | | | NOS Accepted Criteria |
|---|---|---|---|---|---|
| | High Water | | Low Water | | |
| | Amplitude | Time | Amplitude | Time | |
| Difference SM (cm) (min) | 0.9 | 14.5 | 0.4 | 7.2 | na |
| Difference SD (cm) (min) | 1.9 | 5.9 | 2.2 | 4.7 | na |
| RMSE (cm) (min) | 2.1 | 15.7 | 2.2 | 8.6 | na |
| CF (15 cm) (30 min) % | 100 | 99.7 | 100 | 100 | ≥ 90 |
| POF (30 cm) (60 min) % | 0 | 0.3 | 0 | 0 | ≤1 |
| NOF (30 cm) (60 min) % | 0 | 0 | 0 | 0 | ≤1 |
| MDPO (30 cm) (#) | 0 | 0 | 0 | 0 | ≤ 3 |
| MDNO (30 cm) (#) | 0 | 0 | 0 | 0 | ≤ 3 |

**Table 4.6.** Tide simulation high and low water level skill assessment standard statistics at The Battery.

| | The Battery | | | | NOS Accepted Criteria |
|---|---|---|---|---|---|
| | High Water | | Low Water | | |
| | Amplitude | Time | Amplitude | Time | |
| Difference SM (cm) (min) | 4.9 | 18.6 | -9.9 | 11.7 | na |
| Difference SD (cm) (min) | 1.5 | 5.8 | 1.7 | 6.2 | na |
| RMSE (cm) (min) | 5.1 | 19.5 | 10.1 | 13.2 | na |
| CF (15 cm) (30 min) % | 100 | 96.1 | 100 | 100 | ≥ 90 |
| POF (30 cm) (60 min) % | 0 | 0 | 0 | 0 | ≤1 |
| NOF (30 cm) (60 min) % | 0 | 0 | 0 | 0 | ≤1 |
| MDPO (30 cm) (#) | 0 | 0 | 0 | 0 | ≤ 24 |
| MDNO (30 cm) (#) | 0 | 0 | 0 | 0 | ≤ 24 |

## 4.2. Current

### 4.2.1. Harmonic Constants

The longest consecutive ADCP current meter record available within New York Harbor are about 4 months at Bayonne Bridge from January 1 to April 30, 1998. Harmonic constants at bin 8, derived by NOS and at layer 2, derived from the model in the principal current direction (257 degrees true) are listed in Table 4.7. Difference for $M_2$ amplitude is about 7 cm $s^{-1}$, however, the model-based phase lags by 13 degrees, equivalent to about 28 minutes.

**Table 4.7.** Comparison of model-based and NOS accepted current harmonic constants at Bayonne Bridge.

Note: Harmonic constants are in principal current direction 257 degree True.

| | | NOS | | Model | |
|---|---|---|---|---|---|
| | Name | Amp. ($m\ s^{-1}$) | Epoch (degree) | Amp. ($m\ s^{-1}$) | Epoch (degree) |
| 1 | M(2) | 0.789 | 285.6 | 0.851 | 299.0 |
| 2 | S(2) | 0.150 | 329.8 | 0.179 | 338.7 |
| 3 | N(2) | 0.142 | 269.8 | 0.186 | 287.3 |
| 4 | K(1) | 0.051 | 79.5 | 0.063 | 96.4 |
| 5 | M(4) | 0.082 | 185.5 | 0.116 | 268.9 |
| 6 | O(1) | 0.023 | 74.7 | 0.026 | 90.5 |
| 7 | M(6) | 0.066 | 64.9 | 0.084 | 74.7 |
| 8 | MK(3) | 0.000 | 0.2 | 0.000 | 0.2 |
| 9 | S(4) | 0.005 | 46.3 | 0.025 | 18.5 |
| 10 | MN(4) | 0.377 | 37.6 | 0.030 | 18.3 |
| 11 | NU(2) | 0.325 | 83.7 | 0.472 | 58.0 |
| 12 | S(6) | 0.557 | 65.9 | 0.362 | 76.4 |
| 13 | MU(2) | 0.160 | 60.5 | 0.000 | 0.0 |
| 14 | 2N(2) | 0.035 | 4.7 | 0.543 | 37.6 |
| 15 | OO(1) | 0.000 | 0.3 | 0.000 | 0.3 |
| 16 | LAMDA(2) | 0.078 | 33.9 | 0.021 | 27.2 |
| 17 | S(1) | 0.299 | 68.1 | 0.222 | 62.3 |
| 18 | M(1) | 0.000 | 0.0 | 0.006 | 53.1 |
| 19 | J(1) | 0.042 | 34.2 | 0.021 | 36.5 |
| 20 | MM | 0.006 | 98.1 | 0.021 | 36.0 |
| 21 | SSA | 0.000 | 0.0 | 0.023 | 52.3 |
| 22 | SA | 0.000 | 0.4 | 0.000 | 0.4 |
| 23 | MSF | 0.000 | 0.0 | 0.000 | 0.0 |
| 24 | MF | 0.000 | 0.0 | 0.004 | 4.0 |
| 25 | RHO(1) | 0.000 | 0.0 | 0.000 | 0.0 |
| 26 | Q(1) | 0.021 | 1.4 | 0.000 | 0.0 |
| 27 | T(2) | 0.093 | 48.4 | 0.051 | 0.0 |
| 28 | R(2) | 0.000 | 0.0 | 0.153 | 18.4 |
| 29 | 2Q(1) | 0.000 | 0.5 | 0.000 | 0.5 |
| 30 | P(1) | 0.016 | 79.9 | 0.000 | 0.0 |
| 31 | 2SM(2) | 0.024 | 98.6 | 0.019 | 98.6 |
| 32 | M(3) | 0.010 | 48.5 | 0.061 | 36.5 |
| 33 | L(2) | 0.022 | 4.9 | 0.028 | 29.0 |
| 34 | 2MK3(3) | 0.546 | 75.6 | 0.592 | 73.5 |
| 35 | K(2) | 0.156 | 11.0 | 0.283 | 35.5 |
| 36 | M(8) | 0.000 | 0.6 | 0.000 | 0.6 |
| 37 | MS(4) | 0.197 | 97.2 | 0.017 | 25.1 |

### 4.2.2. Skill Assessment for Tidal Current Speed and Direction

Similar to the tide water level skill assessment, the modeled astronomical tidal current speed and direction are compared with predictions from NOS harmonic constants listed in Table 4.7 at the Bayonne Bridge. The entire year 6-minute interval speeds and directions are used in the analysis. Table 4.8 lists the standard suite of skill assessment parameters required by NOS (1999). Only directions with harmonically predicted and modeled speed greater than 26 cm $s^{-1}$ are included in the skill assessment analysis. Tidal current speed has a central frequency of 81.8 %, which is below the NOS accepted criterion of 90%. This is due to the fact that the modeled tidal current lags the predictions, as appeared in the $M_2$ epoch (Table 4.7). This will also show in the time of SBE (slack before ebb) and SBF (slacks before flood), listed in Table 4.9. Besides the speed central frequency, other skill parameters meet NOS accepted criteria by a large margin.

**Table 4.8.** Tide simulation current speed and direction skill assessment standard suit statistics for the entire time series at Bayonne Bridge**.** Note: Predicted: at bin 8, simulated at layer 4, na = not applicable.

| | Speed | | | Direction | | | NOS Accepted Criteria |
|---|---|---|---|---|---|---|---|
| | Predicted | Model | Difference | Predicted | Model | Difference | |
| SM (cm/s) (deg) | 54.1 | 59.9 | 5.9 | 159.1 | 170.5 | 11.4 | na |
| SD (cm/s) (deg) | na | na | 18.9 | na | na | 4.9 | na |
| RMSE (cm/s) (deg) | na | na | 19.8 | na | na | 12.4 | na |
| CF (26 cm/s) (22.5 deg)% | 81.2* | | | 98.9 | | | ≥ 90 |
| POF (52 cm/s)(45 deg) % | 0.6 | | | 0 | | | ≤1 |
| NOF (52 cm/s) (45 deg)% | 0.2 | | | 0.03 | | | ≤1 |
| MDPO (52 cm/s) (45 deg)(Hour) | 0 | | | 0 | | | ≤ 24 |
| MDNO (52 cm/s)(45 deg) (Hour) | 0 | | | 0 | | | ≤ 24 |

### 4.2.3. Skill Assessment for Tidal Current Slack Time

Important information regarding the tidal current in terms of navigation safety is the start and end time of the slack water. This information is important for vessels navigating in a high current channel since it is easier to maneuver during the slack water. The beginning and end times of SBE and SBF time series are obtained from the original uniform-interval harmonically predicted and model-based time series. Two sets of standard NOS suite statistics are then computed based on the differences of SBE and SBF beginning and end times between harmonically predicted and model-based tidal currents.

Table 4.9 indicates that, in general, the simulated time of SBE and SBF lags behind the tide prediction. This can also be seen clearly in the current speed time series, Figure 4.1. Because of the phase lag, many skill statistics do not meet NOS accepted criteria. These statistics are noted with asterisks in the table. The phase lag is much greater for the time of slack before the flood. A possible reason for missing the target is discussed below.

NOS accepted harmonic constants at the Bayonne Bridge are based on data collected between January 1 and April 30, 1998. Due to the complex shallow water interaction in the vicinity of measurement and the flow regimes between Newark Bay, Kill Van Kull, and Arthur Kill, a phase lag during SBF exists in the harmonically predicted tidal current when compared with observations. The model simulated tidal current accuracy could be improved by adjusting the shoreline location or other model parameters without increasing grid resolution. However, this process could be very time consuming since many sensitivity tests would be needed. At present, we continue to work on this improvement in order to be closer to the NOS accepted criteria.

**Table 4.9.** Skill assessment standard suite statistics for tidal current beginning and end time of SBE (slack before ebb) and SBF (slack before flood) differences between harmonically predicted (at bin 8) and simulated currents (at layer 4) at the Bayonne Bridge. Note: na = not applicable

| | SBE | SBF | NOS Accepted Criteria |
|---|---|---|---|
| SM (minutes) | 30.7 | 35.4 | na |
| SD (minutes) | 20.6 | 12.5 | na |
| RMSE (minutes) | 36.9 | 37.5 | na |
| CF (15 minutes) % | 27.5* | 2.9* | ≥ 90 |
| POF (30 minutes) % | 47.9* | 67.6* | ≤1 |
| NOF (30 minutes) % | 0 | 0.2 | ≤1 |
| MDPO (30 minutes) (#) | 0 | 33* | ≤ 24 |
| MDNO (30 minutes) (#) | 0 | 0 | ≤ 24 |

## 5. MODEL HINDCASTS

Results reported in Chapter 4 show good comparisons between model-simulated and harmonically predicted tides and tidal currents. The model is then validated with observed total water levels and currents over a period from January 1 to December 31, 1997. The purpose of this simulation is two-fold; validating hydrodynamic parameters used in the model and assessing the model skill at handling the meteorological and hydrological effects. Both the one- and two-way coupled models described in Chapter 3 are used for the simulation in order to evaluate if there is an accuracy improvement in the nested grid and the two-way coupling technique. However, the skill assessment is performed based on the results from the one-way coupled model.

### 5.1. Boundary Conditions

Water level observations at Sandy Hook, NJ, and Willets Point, NY, are used as model lateral open boundary conditions. The model is also forced at the surface with surface winds and atmospheric pressure from Buoy 44025 near the harbor entrance. Figure 5.1 shows the water levels at Sandy Hook and Willets Point and the hourly buoy wind stresses and atmospheric pressure for January, 1997. The water level time series show that the semidiurnal tide dominates, with more than 1.7 m spring tide range at Sandy Hook and 2.0 m at Willets Point. In addition to the astronomical tide, the meteorological effects on the water level are clear during a storm moving through the area around January 7. Mean water level decreased at both locations due to the eastward wind blowing offshore. On January 10, the atmospheric pressure dropped to 991 mb due to the storm center moving into the area. Mean water levels increased due to strong westward winds (up to 16 dyne $cm^{-2}$) associated with the low pressure center. Wind direction then returned to eastward after the storm center passed and the water level was lowered. This illustrates the coastal meteorological effect on the water levels at Willets Point and Sandy Hook, which in turn influences the water levels in the harbor.

Monthly mean river discharges (Figure 5.2) based on 1988 to 1997 United States Geological Survey (USGS) daily mean flow at four rivers: Raritan (Sta. No: 01403060, below Calco Dam at Bound Brook, NJ), Passaic (Sta. No: 01389500, Little Falls, NJ), Hackensack (Sta. No: 01377000, at Riverdale, NJ), and Hudson Rivers (Sta. No: 01335754, above Lock 1, near Waterford, NY), are specified as inflow to the model grid. The Hudson River is the major freshwater tributary in this estuarine system with mean discharges reaching 470 $m^3 s^{-1}$ in the spring. Discharges from the Raritan and Passaic Rivers account for only 20% of the Hudson River mean flow. Tests show that although river discharges may modify the tidal current phase near the eastern entrance to the Kill Van Kull, the effects on the water levels in the bay are minor when compared to the coastal meteorological effects.

### 5.2. Results

Figure 5.3 shows the comparison between simulated water levels and observations at the Bayonne Bridge and The Battery (Fig. 1). Simulated water levels show no significant difference between the coarse and fine grids at both locations. In addition, simulated water levels at the Bayonne Bridge from the one- and two-way coupling models are very similar, indicating the model nesting and

coupling technique have insignificant impact on simulated water levels. However, the impact of grid resolution and the coupling technique on the current speed is apparent.

Figure 5.4 shows two current meter locations near the Bayonne Bridge and Bergen Point. The Bergen Point ADCP (Acoustic Doppler Current Profiler) recorded valid measurements during January and February 1997while the current meter at the Bayonne Bridge recorded valid measurements from January to June 1997. There was a period about 40 days when both current meters were working simultaneously. Figures 5.5 and 5.6 show observed and simulated current speed time history at Bayonne Bridge and Bergen Point. Model results shown in the figures are at layers 2 and 3 (about 3 and 5 m from water surface) from 3 cases: coarse grid, one-way coupling fine grid, and two-way coupling fine grid. Observations are taken from bin 9 and bin 7 at depths corresponding to model layers 2 and 3. For a better comparison, the observed currents have been low-pass filtered to smooth out high frequency signals less than 90 minutes. The current speed and current patterns during flood and ebb are quite different between two locations. The ebb current speed is much less than the flooding current speed at Bergen Point. In general, simulated maximum current speed from the coarse grid (dotted line) is less than that from the fine grid at both locations perhaps due to lack of fine scale resolution, particularly at Bergen Point (Fig. 5.6). Current speeds from the one- and two-way coupling schemes show insignificant differences at both locations. At the Bayonne Bridge (Fig. 5.5), the model under-predicts the current during the flood and over-predicts during the ebb.

## 5.3. Skill Assessment

The simulated water levels and currents are compared with observations to evaluate the model skill according to the procedures and statistic parameter requirements described in NOS (1999). The purpose is to evaluate if the model is accurate for water level and current predictions. The water level and current are assessed separately. For water level skill assessment, the complete simulated and observed hourly time series as well as the high and low water time series, are analyzed to obtain the standard suite of statistical parameters. For the currents, the simulated and observed 6-minute interval speed and direction information are used for standard suite of statistical parameters. The slack time statistics, involving the beginning and end time of the slack current, are also obtained according to NOS (1999).

### 5.3.1. Skill Assessment for Water Levels

Table 5.1 lists the standard suite of statistics for water levels at the Bayonne Bridge and The Battery. Hourly observed and model data at Bayonne Bridge for 12 months in 1997 are used, however, only four months (January to April in 1997) of data at The Battery are used due to the observed data quality problem from May to December (William Stoney, NOS, personal communication). The acceptable criteria recommended by NOS are also included in the table. All the model statistical parameters are within NOS acceptable range. The simulated mean water level (MWL) is higher than the observed MWL at the Bayonne Bridge by 2.3 cm, however, lower at The Battery by 1.2 cm. Monthly MWL at Sandy Hook, Willets Point, Bayonne Bridge, and The Battery are shown in Figure 5.7. Apparently, the high monthly MWL at the Bayonne Bridge and The Battery for April results

from MWL at Sandy Hook. However, unusual high observed MWL at The Battery occurs from May to November due to data error. Average MWL for the entire coarse grid domain is also shown in Figure 5.7. The entire domain average MWL is very close to the values at Sandy Hook, except in November, indicating that there is only a small portion of the net inflow influence from Willets Point through East River to the Harbor.

### 5.3.2. Skill Assessment for High and Low Water Levels

A standard suite of assessment statistics for amplitude and time of high and low water are computed for the Bayonne Bridge and The Battery. Simulated water levels at the Bayonne Bridge and The Battery are taken from the fine grid and coarse grid, respectively. The high and low water time series subsets are derived from the entire 6-minute interval simulated and observed water level time series and the differences are computed. The standard suite of statistical parameters are derived and listed in Tables 5.2 and 5.3. All statistical parameters at the Bayonne Bridge are within NOS accepted criteria; however, CF (84.9%) and POF (1.3%) of high water time at The Battery are slightly below the threshold. Simulated high and low water time lag behind the observations about 20 minutes at both locations. The mean model high and low water amplitudes are higher than the observations, except for the low water amplitude at The Battery.

### 5.3.3. Skill Assessment for Current Speed and Direction

Current observations in bin 7 (about 5 m below water surface) are compared with simulated current speed and direction in layer 3 (also about 5 m below the water surface) at the Bayonne Bridge over 5 months from January 17 to June 19, 1997. Because there are 3 gaps in the observed data over this 5 month period, the entire data set has been separated into 4 continuous data sets, resulting in 29,806 total valid 6-minute interval data, equivalent to about 4 months. The simulated currents are interpolated to the observed data time to make one-to-one comparisons. The parameters in the analysis are obtained based on the entire data set except for MDPO and MDNO (maximum duration of positive/negative outliers), which are based on each continuous data set.

Current speed and direction skill assessments for the Bayonne Bridge are listed in Table 5.4. The current speed CF (82.8%) is slightly below the NOS acceptable criterion (90%). Other parameters are either close to or within the NOS acceptable values. The speed RMS error of about 19 cm $s^{-1}$ is mostly due to the phase lag of simulated current speed. This can also be seen in the SBF and SBE slack time analysis results presented in Table 5.6.

Available current speed and direction observations (bin 7 for observations and layer 3 for simulated) at Bergen Point were only half of those at Bayonne Bridge. About 14,156 continuous 6-minute interval data are used in the analysis, and the result is listed in Table 5.5. The skill is not as good as Bayonne Bridge, probably due to the complicated flow pattern in the area.

### 5.3.4. Skill Assessment for Current Slack Time

Similar to the astronomical simulation, the skill assessment for the beginning and end time of SBE and SBF series are computed. First, the beginning and end time of SBE and SBF are obtained from the observed and uniform-interval model based time series. Two sets of standard NOS statistics are then computed based on the differences of SBE and SBF beginning and end times between observed and model-based tidal currents. Table 5.6 lists the statistical parameters for Bayonne Bridge. Although the model performance is below NOS acceptable criteria, the statistics are still better than the results from the tidal simulation (Table 4.9). The skills of CF, POF, and NOF have been improved dramatically, although still below the criteria, when the criteria was doubled (relaxed) (below the double line in Table 5.6). Due to the complex flow patterns and shears near Bergen Point, it is very difficult to define SBE and SBF based on a single pre-specified current speed. Therefore, the slack time analysis is not performed at this location.

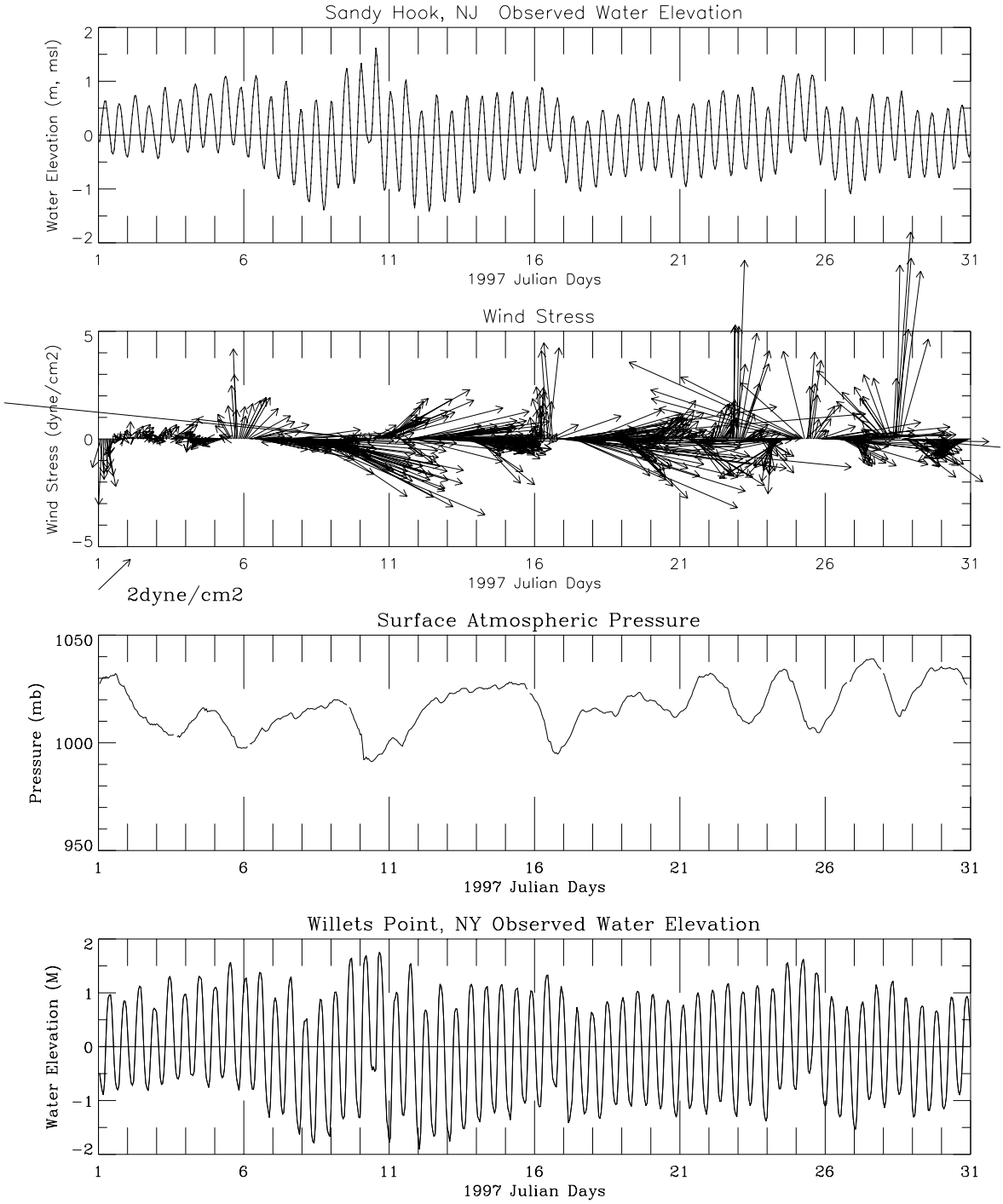


**Figure 5.1.** Observed water surface elevations at Sandy Hook, NJ and Willets Point, NY for January, 1997, and surface wind stresses and atmospheric pressure from Buoy 44025.

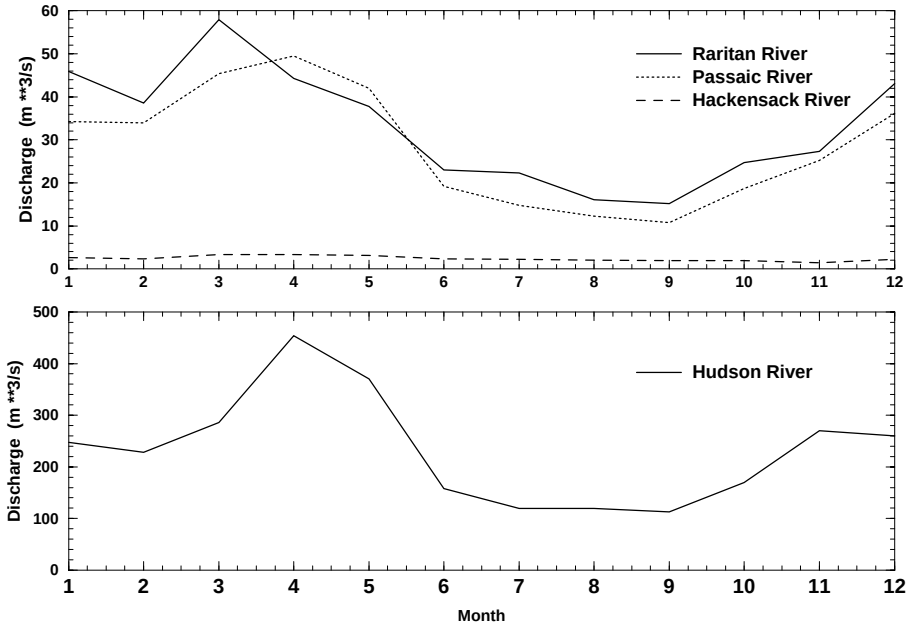


**Figure 5.2.** Monthly averaged flow at Raritan, Passaic, Hackensack, and Hudson Rivers, based on USGS daily averaged flow from 1988 to 1997.

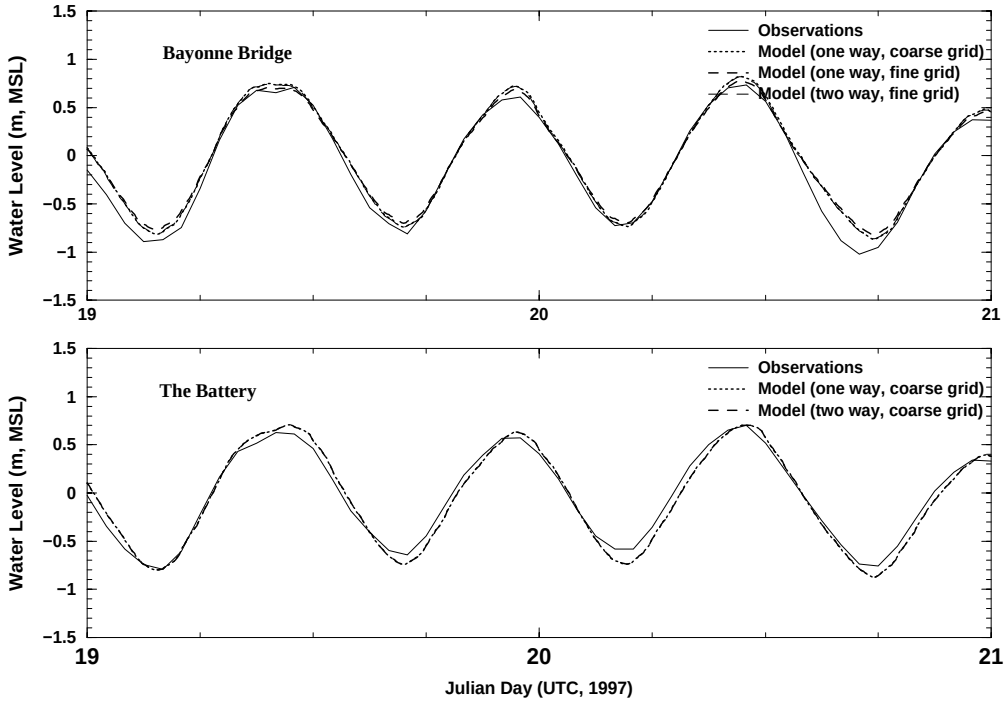


**Figure 5.3.** Simulated water levels from coarse and fine grids and one- and two- way coupling models compared with observations at Bayonne Bridge (top) and The Battery (bottom).

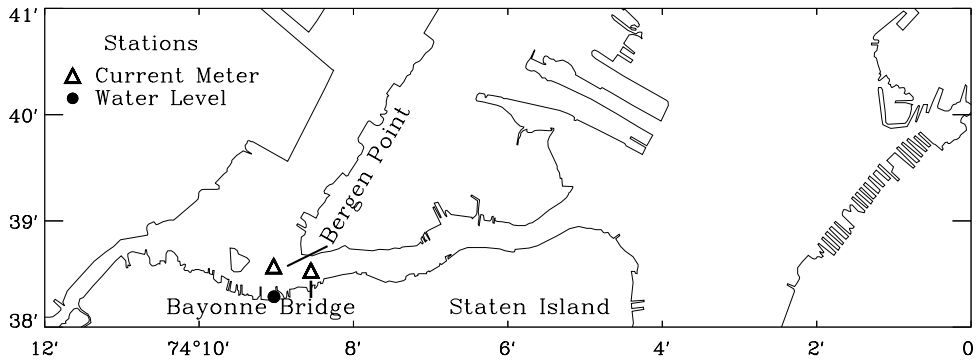


**Figure 5.4.** Current meter locations at Bergen Point and Bayonne Bridge for 1997 simulation.

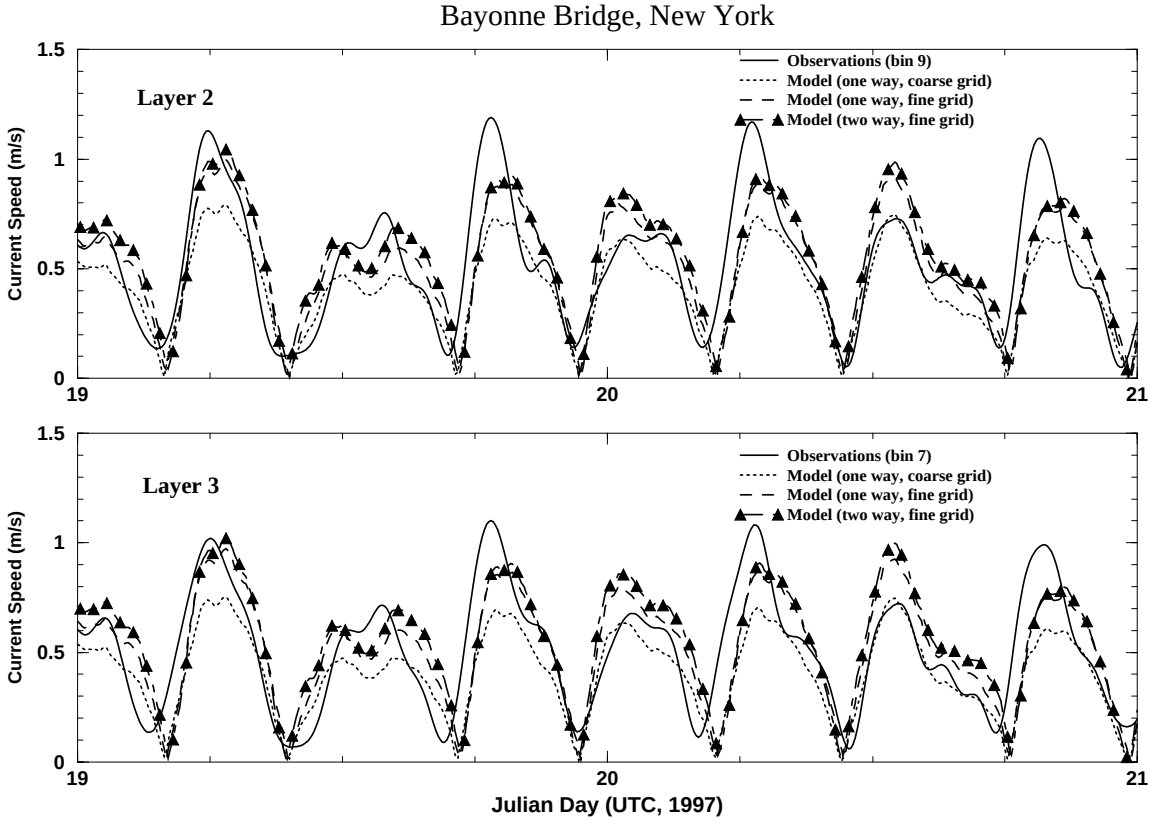


**Figure 5.5.** Simulated current speed from coarse and fine grids and one- and two- way models compared with observations at Bayonne Bridge. Layer 2 (top) and 3 (bottom) are about 3 m and 5 m below water surface, respectively.

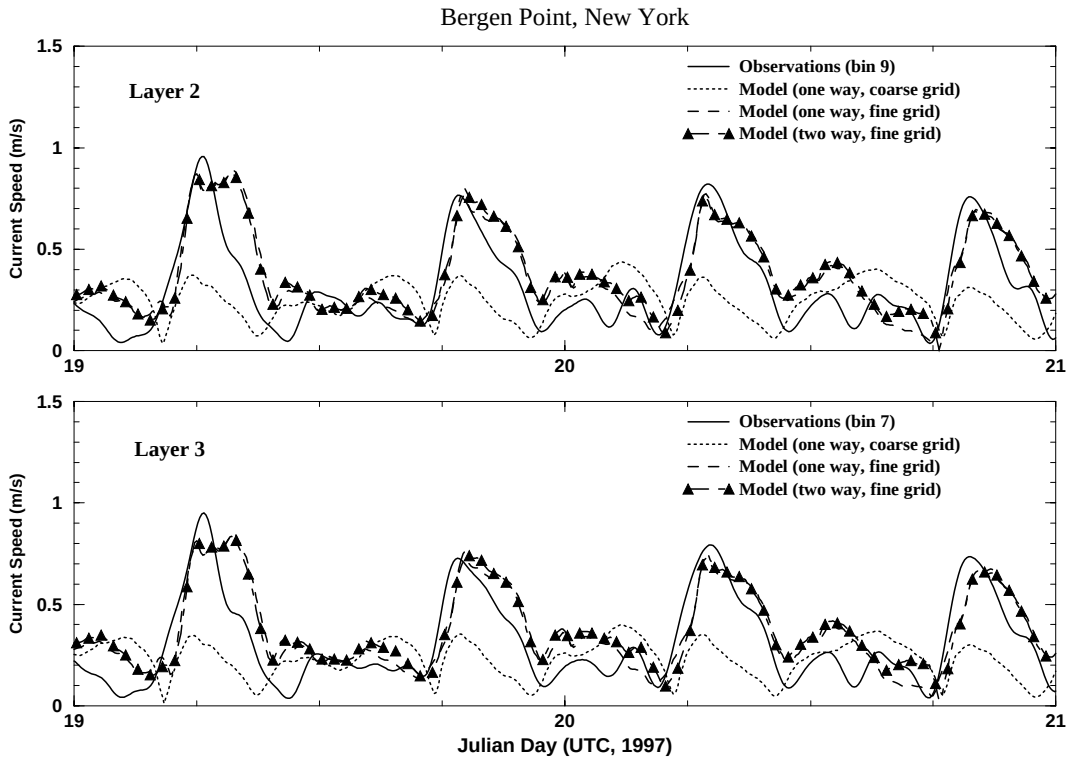


**Figure 5.6.** Simulated current speed from coarse and fine grids and one- and two- way models compared with observations at Bergen Point. Layer 2 (top) and 3 (bottom) are about 3 m and 5 m below the water surface, respectively.

**Table 5.1.** Water level hindcast skill assessment standard statistics for complete time series at Bayonne Bridge and The Battery. (Note: na = not applicable)

| | Bayonne Bridge | | | The Battery | | | NOS Accepted Criteria |
|---|---|---|---|---|---|---|---|
| | Observed | Model | Difference | Observed | Model | Difference | |
| SM (cm) | 7.6 | 9.9 | 2.3 | 8.0 | 6.8 | -1.2 | na |
| SD (cm) | na | na | 8.2 | na | na | 9.2 | na |
| RMSE (cm) | na | na | 8.6 | na | na | 9.3 | na |
| CF (15 cm) % | 91.5 | | | 90.9 | | | ≥ 90 |
| POF (30 cm) % | 0.7 | | | 0.1 | | | ≤1 |
| NOF (30 cm) % | 0.1 | | | 0.2 | | | ≤1 |
| MDPO (30 cm) (Hour) | 7 | | | 1 | | | ≤ 24 |
| MDNO (30 cm) (Hour) | 2 | | | 3 | | | ≤ 24 |

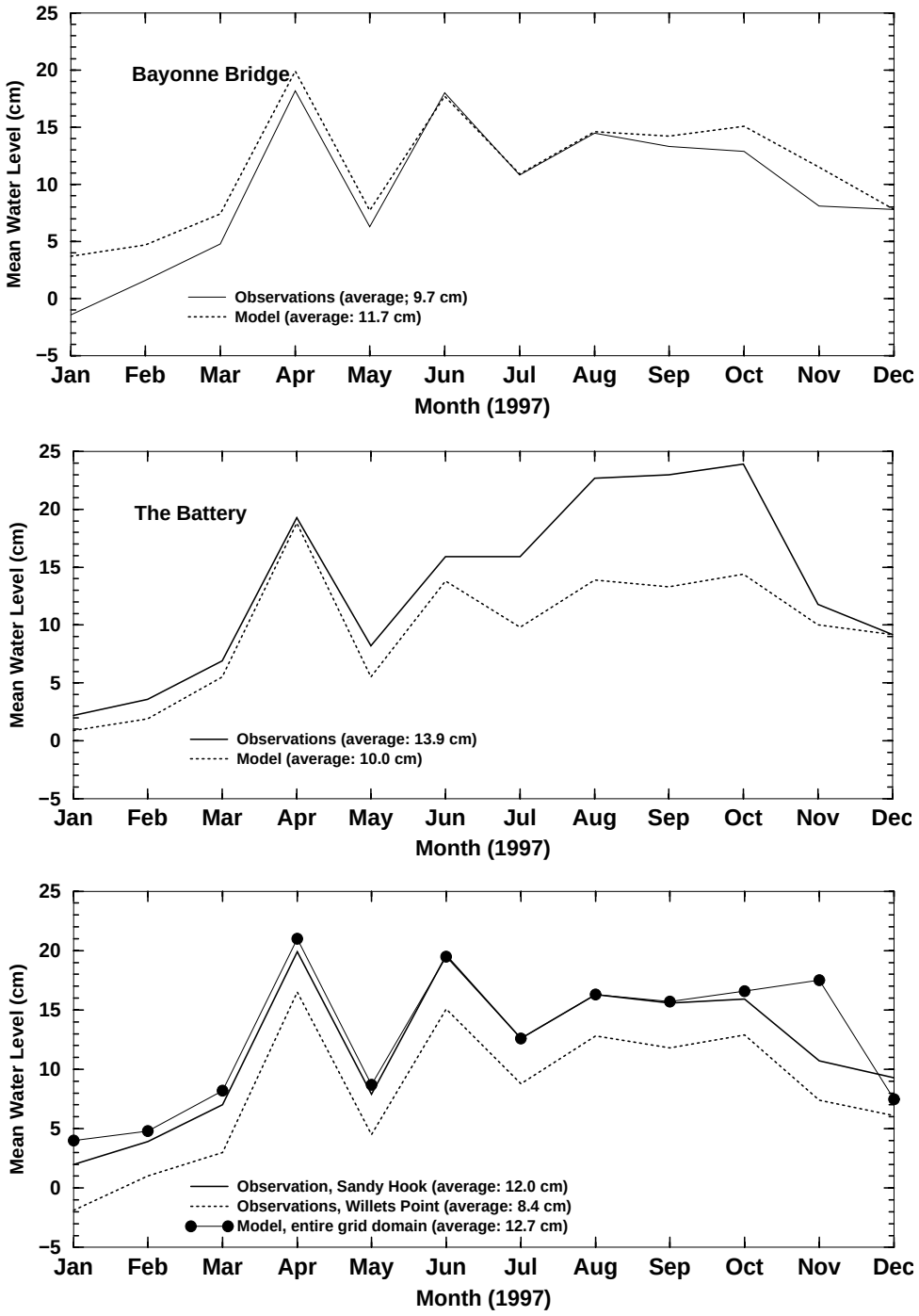


**Figure 5.7.** Monthly mean (for 1997) water level for observations at Sandy Hook, Willets Point, Bayonne Bridge, and The Battery and for the model at the Bayonne Bridge, The Battery, and the entire coarse grid domain.

**Table 5.2.** High and low water level hindcast skill assessment standard suite statistics at the Bayonne Bridge. (Note: na = not applicable)

| | Bayonne Bridge | | | | NOS Accepted Criteria |
|---|---|---|---|---|---|
| | High Water | | Low Water | | |
| | Amplitude | Time | Amplitude | Time | |
| Difference SM (cm) (min) | 3.0 | 6.9 | 5.4 | 0.8 | na |
| Difference SD (cm) (min) | 5 | 17.5 | 6.9 | 17 | na |
| RMSE (cm) (min) | 5.8 | 18.8 | 8.7 | 17 | na |
| CF (15 cm) (30 min) % | 97.2 | 90.6 | 91.9 | 94.3 | ≥ 90 |
| POF (30 cm) (60 min) % | 0.1 | 0.7 | 1 | 0 | ≤1 |
| NOF (30 cm) (60 min) % | 0 | 0.1 | 0 | 0.6 | ≤1 |
| MDPO (30 cm) (#) | 1 | 1 | 2 | 0 | ≤ 3 |
| MDNO (30 cm) (#) | 0 | 1 | 0 | 1 | ≤ 3 |

**Table 5.3.** High and low water level hindcast skill assessment standard suite statistics at The Battery. (Note: na = not applicable)

| | The Battery | | | | NOS Accepted Criteria |
|---|---|---|---|---|---|
| | High Water | | Low Water | | |
| | Amplitude | Time | Amplitude | Time | |
| Difference SM (cm) (min) | 5.2 | 12.5 | -6.1 | 4.5 | na |
| Difference SD (cm) (min) | 5.5 | 18.4 | 6.5 | 16.4 | na |
| RMSE (cm) (min) | 7.5 | 22.2 | 8.9 | 17.1 | na |
| CF (15 cm) (30 min) % | 96.6 | 84.9* | 96.1 | 92.4 | ≥ 90 |
| POF (30 cm) (60 min) % | 0.4 | 1.3* | 0 | 0 | ≤1 |
| NOF (30 cm) (60 min) % | 0 | 0 | 0 | 0 | ≤1 |
| MDPO (30 cm) (#) | 1 | 1 | 0 | 0 | ≤ 24 |
| MDNO (30 cm) (#) | 0 | 0 | 1 | 0 | ≤ 24 |

**Table 5.4.** Current speed and direction hindcast skill assessment standard suite statistics at Bayonne Bridge, based on 29,806 six minutes interval data. (Note: na = not applicable)

| | Speed | | | Direction | | | NOS Accepted Criteria |
|---|---|---|---|---|---|---|---|
| | Observed | Model | Difference | Observed | Model | Difference | |
| SM (cm/s) (deg) | 53.6 | 56.8 | 3.2 | 183.9 | 174.2 | -9.7 | na |
| SD (cm/s) (deg) | na | na | 18.8 | na | na | 23.6 | na |
| RMSE (cm/s) (deg) | na | na | 19.1 | na | na | 25.6 | na |
| CF (26 cm/s) (22.5 deg)% | 82.8 | | | 93.3 | | | ≥ 90 |
| POF (52 cm/s)(45 deg) % | 1.1 | | | 0.4 | | | ≤1 |
| NOF (52 cm/s) (45 deg)% | 0.5 | | | 1.4 | | | ≤1 |
| MDPO (52 cm/s) (45 deg)(Hour) | 1.5 | | | 1.4 | | | ≤ 24 |
| MDNO (52 cm/s)(45 deg) (Hour) | 1.7 | | | 0.9 | | | ≤ 24 |

**Table 5.5.** Current speed and direction hindcast skill assessment standard suite statistics at Bergen Point, based on 14,158 six minutes interval data. (Note: na = not applicable)

| | Speed | | | Direction | | | NOS Accepted Criteria |
|---|---|---|---|---|---|---|---|
| | Observed | Model | Difference | Observed | Model | Difference | |
| SM (cm/s) (deg) | 31.1 | 41.5 | 10.4 | 278.3 | 271.9 | -6.4 | na |
| SD (cm/s) (deg) | na | na | 18.5 | na | na | 46.4 | na |
| RMSE (cm/s) (deg) | na | na | 21.2 | na | na | 46.8 | na |
| CF (26 cm/s) (22.5 deg)% | 83.9 | | | 77.3 | | | ≥ 90 |
| POF (52 cm/s)(45 deg) % | 3.6 | | | 1.6 | | | ≤1 |
| NOF (52 cm/s) (45 deg)% | 0.1 | | | 6.1 | | | ≤1 |
| MDPO (52 cm/s) (45 deg)(Hour) | 2.5 | | | 0.7 | | | ≤ 24 |
| MDNO (52 cm/s)(45 deg) (Hour) | 0.5 | | | 1.9 | | | ≤ 24 |

**Table 5.6.** Skill assessment standard suite statistics for begin and end times of SBE (slack before ebb) and SBF (slack before flood) differences between observed (at bin 7) and simulated currents (at layer 3) at Bayonne Bridge. (Note: na = not applicable)

| | Bayonne Bridge | | |
|---|---|---|---|
| | SBE | SBF | NOS Accepted Criteria |
| SM (minutes) | 8.5 | 24.0 | na |
| SD (minutes) | 26.0 | 26.0 | na |
| RMSE (minutes) | 27.4 | 36.1 | na |
| CF (15 minutes) % | 46.0 | 17.6 | ≥ 90 |
| POF (30 minutes) % | 19.3 | 38.4 | ≤1 |
| NOF (30 minutes) % | 5.3 | 3.1 | ≤1 |
| CF (30 minutes) % | 75.4 | 58.5 | |
| POF (60 minutes) % | 1.8 | 3.8 | |
| NOF (60 minutes) % | 0.7 | 1.6 | |

## 6. SUMMARY

The Port of NY/NJ water level and current nowcast/forecast model has been developed based on the three-dimensional barotropic Princeton Ocean Model. The purpose of developing this model is for water level and current predictions within the New York Harbor. The model will be the core component within the nowcast/forecast system which utilizes NOS PORTS information to provide near real-time nowcast information. With proper water level forecasts at Sandy Hook and Willets Point such as from NWS's ETSS (Extra Tropical Storm Surge), wind stress forecasts such as NWS's Eta, and river flow forecasts, the system will also provide short term forecasts to mariners including ship pilots and the Coast Guard for optimizing ship operation, navigation safety, and vessel traffic control.

The model includes a fine grid, which covers the Upper Bay, the Kill Van Kull, and Newark Bay, nested within the coarse grid. The coupling technique, developed in this study, allows water levels and momentum fluxes to be communicated between the two grids through the grid interface. The model code uses a common block to store the interface information so that no external data files are required for model information exchange and the two models are running within one executable code. The model has been calibrated for tidal simulations and assessed with long term observed water levels and currents spanning over various time scales from tidal to seasonal cycles. The model simulations show insignificant differences for water levels between the fine grid and the coarse grid. However, the fine grid is more accurate in simulating currents than the coarse grid due to a higher grid resolution and more detailed shore and bathymetry representation. Experiments also show that the simulated current differences between one- and two- way coupling are insignificant. Therefore, the one-way coupling model will be used in the proposed operational nowcast/forecast model system.

The barotropic POM model used in the system does not include the effects of density. Therefore, for the simulated circulation, the bottom friction is the primary factor responsible for the vertical velocity structure due to lack of density stratification. Industrial ship operation requires the density information for maximizing the cargo draft. In the near future the barotropic model will be extended to include the salinity and temperature. The salinity and temperature information will not only be useful for navigation safety and the economy but also the key information input for water quality and environmental requirements.

## ACKNOWLEDGMENTS

The development of Port of New York/New Jersey water level and current nowcast/forecast model system has been carried out at Coast Survey Development Laboratory (CSDL) of NOS's Office of Coast Survey under the leadership of CSDL's Chief Dr. Bruce Parker. Dr. Parker suggested the development of nested grid model in resolving detail current pattern and structure in the Kill Van Kull for the navigation purpose. The second author Manchun Chen, a visiting scientist at CSDL from National Marine Data Information Service (NMDIS) of Peoples Republic of China's (PRC) State Oceanographic Agency (SOA), developed the nested grid model coupling technique. We thank

Dr. Leo Oey of Princeton University for providing guidance in the model nesting technique development. Dr. Frank Aikman, Chief of CSDL's Marine Modeling and Analysis Programs (MMAP) has provided valuable comments to the project. His critical report review is acknowledged. Dr. Aijun Zhang, also a visiting scientist from NMDIS, is also acknowledged for his assistance in performing many model sensitivity experiments.

## REFERENCES

Bethem, T.D. and H.R. Frey, 1991. Operational Physical Oceanographic Real-Time Data Dissemination. In **Proc. IEEE OCEANS** '91, 1991, p.864.

Blumberg, A.F., and G.F. Mellor, 1987. A Description of a Three-dimensional Coastal Ocean Circulation Model. In: **Three-dimensional Coastal Ocean Models**, Coast and Estuarine Science, Vol. 4 (Heaps, N.S. ed.), American Geophysical Union, Washington, D.C., 1-16.

Jones, R. W., 1977. Noise Control for a Nested Grid Tropical Cyclone Model. **Atmos. Phys**., **50**, 393-402.

Oey, L.-Y., and P. Chen, 1992. A Nested Grid Ocean Model: With Application to the Simulation of Meanders and Eddies in the Norwegian Coastal Current. **J. Geophys. Res**., **97**, 20,063-20,086.

Mellor, G.L., 1998. Users Guide for A Three-Dimensional, Primitive Equation, Numerical Ocean Model. Program in Atmospheric and Oceanic Sciences, Princeton University, 41p.

National Ocean Service (NOS), 1999. NOS Procedure for Developing and Implementing Operational Nowcast and Forecast System for PORTS. **NOAA Technical Report**, NOS CO-OPS 0020, NOAA/NOS, 33p.

Parker, B.B., 1996. Monitoring and Modeling of Coastal Waters in Support of Environmental Preservations. **J. Mar. Sci. Technol**., **1**, 75-84.

Schureman, P., 1971. Manual of Harmonic Analysis and Prediction of Tides. U.S. Govt. Print. Off., U.S. Coast and Geodetic Survey, **Special Publication** 98. 317 pp.

Wei, E.J., M. Chen, and A. Zhang. 1998. Development of a New York/New Jersey Harbor Water Level and Current Nowcast/Forecast System. **Proceedings, Ocean Community Conference '98**, Baltimore, Maryland, 16-19, 1998. p422-425.

Zervas, C., 1999. Tidal Current Analysis Procedures and Associated Computer Programs. **NOAA Technical Report** NOS CO-OPS 0021. 101 pp.

Zhang, D.-L., and H.-R. Chang, 1986. A Two-way Interactive Procedure with Variable Terrain Resolution. **Monthly Weather Review**, **114**, 1330-1339.